American Mineralogist, Volume 81, pages 429–447, 1996

Parameterization of energy and interactions in garnets: End-member properties

G. Ottonello,[1] M. Bokreta,[2] and P.F. Sciuto[1]

[1]Department of Earth Sciences, University of Genoa, Corso Europa 26, 16132 Genoa, Italy
[2]University of Pennsylvania, 3465 Sansom Street, Philadelphia, Pennsylvania 19104, U.S.A.

Abstract

We present results of static lattice energy and vibrational energy calculations for the 12 garnet end-members in the system $(Ca,Mg,Mn,Fe)_3(Al,Cr,Fe)_2Si_3O_{12}$. The structure of the end-member phases was first simulated with the aid of expressions of the Novak-Gibbs type followed by a distance least-squares treatment (DLS), with an appropriate choice of the ionic radii of the cations in the crystal structure. The high-P garnet structure was simulated with the assumption that cation-to-O distances obey the generalizations of Hazen and Finger (1979, 1982). Polyhedral compressibilities were modified to account for the P dependency of bulk modulus. The resulting bulk moduli are in satisfactory agreement with experimental observations and are internally consistent. The thermal expansion of the various end-members was derived from linear polyhedral expansivities, in a fashion analogous to that used to determine compressibility, by structural simulation and DLS refinements.

Compressibilities of garnet end-members are shown to be consistent with the usual exponential form of short-range pair potentials, with a hardness factor ranging from 0.45 to 0.51 Å and averaging approximately 0.48 Å. Adopting the Huggins-Mayer formulation of repulsive terms (constant hardness factor $\rho = 0.48$ for the family of isostructural compounds) and assuming initially repulsive radii to be equal to the crystal radii, it is shown that the preexponential b factors closely obey the Born-Mayer generalization (repulsive factor, b, constant in the same family of compounds). Static energies of the common compounds were then solved with the assumption of full ideality (i.e., ρ and b constant in the family of isostructural salts) and for the appropriate repulsive radii. Because the static energies of the 12 garnet end-members are rigorously coplanar in the chemical space of interest, in light of the Born-Haber-Fayans thermochemical cycle, the repulsive energies of the six uncommon end-members (hence the bulk static energy and the corresponding enthalpy at reference state) were readily obtained by application of the combined Huggins-Mayer and Born-Mayer approach. Heat capacities and entropies for all end-members were determined by following the guidelines of the Kieffer model, adjusting the lower cut-off frequency of the optical continuum $\omega_{l,K_{max}}$ such that the calorimetric third-law entropy (after correction for anharmonicity and magnetic spin) is reproduced and at the same time conforming to the low-T C_P calorimetric data. A complete set of thermodynamic parameters is given for all 12 garnet end-member components.

Introduction

Garnets have been a subject of intense investigation, mainly because of their importance in influencing mantle chemistry and their thermobarometric implications in solid ⇌ solid equilibria. Both types of study require, however, an internally consistent and complete data set to avoid error-progression effects such as those described by Kohn and Spear (1991). In this paper we examine the implications for the garnet database arising from interionic static potential calculations and from vibrational calculations. The garnets considered in this study are confined to the system $(Ca,Mg,Mn,Fe)_3(Al,Cr,Fe)_2Si_3O_{12}$. Twelve end-members occur in the system (Table 1). Pure end-members are nonexistent in nature, but all of them have been synthesized in the laboratory. The first six garnets in Table 1 are denoted here as "common" garnets and make up the aluminous group and the calcic group. Most of the physical and thermochemical investigations were focused on these groups. The last six garnets in the table are termed "uncommon" garnets because they are present only in small proportions in natural compounds or not found at all (e.g., iron chromium garnet and manganese chromium garnet; Fursenko 1981). Thermochemical data are lacking for the members of this group. However, interest in them has increased, especially because of the role played by knorringite in mantle-garnet solid mixtures (Irifune et al. 1982). Moreover, calderite and khoharite are present in the modal compositional representation of some high-pressure garnets (Rickwood 1969;

0003-004X/96/0304-0429$05.00

TABLE 1. Garnet end-members in the system $(Ca,Mg,Mn,Fe)_3(Al,Cr,Fe)_2Si_3O_{12}$ and refinements for garnet compounds under various *T-P* conditions

Name	Ref. no.	Formula	Ref. (lattice param.)
Pyrope	1	$Mg_3Al_2Si_3O_{12}$	a
Almandine	2	$Fe_3Al_2Si_3O_{12}$	b
Spessartine	3	$Mn_3Al_2Si_3O_{12}$	b
Grossular	4	$Ca_3Al_2Si_3O_{12}$	a
Uvarovite	5	$Ca_3Cr_2Si_3O_{12}$	c
Andradite	6	$Ca_3Fe_2Si_3O_{12}$	a
Knoringite	7	$Mg_3Cr_2Si_3O_{12}$	d
Calderite	8	$Mn_3Fe_2Si_3O_{12}$	e
Skiagite	9	$Fe_3Fe_2Si_3O_{12}$	f
Khoharite	10	$Mg_3Fe_2Si_3O_{12}$	g
Manganese chromium garnet	11	$Mn_3Cr_2Si_3O_{12}$	h
Iron chromium garnet	12	$Fe_3Cr_2Si_3O_{12}$	h
End-members (room *T-P*)			
Pyrope			i, j, a, k
Almandine			l, k, m
Grossular			n, o, a
Andradite			p, a, q
Crystals at high *P*			
Pyrope			r, s, t
Spessartine			r, s
Andradite			r, s, t
Grossular			s, r
Crystals at high *T*			
Pyrope			u, v
Grossular			u
Andradite			v

Note: References are as follows: a = Novak and Gibbs (1971), b = Skinner (1956), c = Hukenholtz and Knittel (1975), d = Irifune et al. (1982), e = Lattard and Schreyer (1983), f = Karpinskaya et al. (1983), g = McConnell (1966), h = Fursenko (1981), i = Zemann and Zemann (1961), j = Gibbs and Smith (1965), k = Armbruster et al. (1992), l = Prandl (1971), m = Woodland and O'Neill (1993), n = Abraham and Geller (1958), o = Prandl (1966), p = Quareni and De Pieri (1966), q = Woodland and Ross (1994), r = Meagher (1975), s = Rakai (1975), t = Hazen and Finger (1989), u = Hazen and Finger (1978), and v = Armbruster and Geiger (1993).

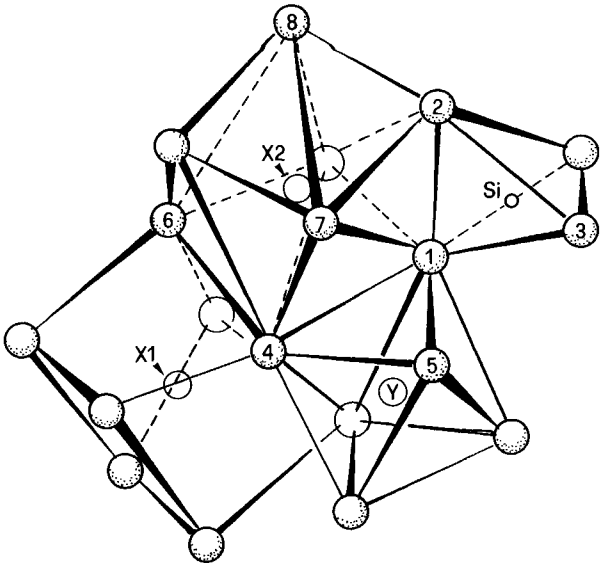

FIGURE 1. Part of the unit cell of garnets showing equivalent distances utilized in the structural simulation and the adopted O labeling.

Sobolev 1974). The presence of these uncommon garnets in natural mixtures makes it important to account for their energy contributions as components of a solid mixture.

Since Menzer (1926) established the crystal structure of garnets, several determinations and refinements have been made (Table 1). The garnet type structure is described by the *Ia3d* space group. Its body-centered cell contains eight formula units of the form $X_3Y_2Z_3O_{12}$, where *X*, *Y*, and *Z* are cations occupying the special positions *c*, *a*, and *d*, respectively, with no degrees of freedom, whereas O anions are in the general position *h*, with three degrees of positional freedom (in this study *X* is divalent, *Y* is trivalent, and $Z = Si^{4+}$). The arrangement of the O anions around the *X*, *Y*, and *Z* cations forms three types of coordination polyhedra (Fig. 1): a dodecahedron around the *X* cation, an octahedron around *Y*, and a tetrahedron around *Z*. The labeling of the ions adopted here in identifying the nonequivalent distances in the asymmetric unit (Si-O, *Y*-O, *X*1-O, *X*2-O, O1-O2, O1-O4, O1-O5, O1-O7, O4-O6, O4-O7, and O7-O8) is that of Novak and Gibbs (1971), which was also followed by Meagher (1975), Hazen and Finger (1978), and Basso (1985) (Table 2).

SIMULATION OF GARNET STRUCTURE UNDER DIFFERENT *P-T* CONDITIONS

Gnevushev et al. (1956) estimated the lattice parameter of garnets from the type of cations present in the structure. Since then, many other linear regression equations have been proposed, such as that of Bertaut and Forrat (1957) using Goldschmidt radii, McConnell (1966) using Arens radii, and Novak and Gibbs (1971) using Shannon and Prewitt (1969) radii. Novak and Gibbs (1971), using multiple regression analysis, derived linear equations giving the O positional parameters as a function of the *X*, *Y*, and *Z* cation radii. This method was later extended by Hawthorne (1981) to many oxide garnets, and by Basso (1985) to hydroxide garnets. In this study, we use Basso's equation relating the crystallographic parameters to the chemical compositions to predict the lattice parameter, the O positional parameters, and the nonequivalent distances in the asymmetric unit. As shown in Table 2, both the O positional parameters and the nonequivalent distances in the asymmetric unit may be expressed as functions of the mean cation radii in the *X*, *Y*, and *Z* sites. The lattice parameter is expressed as a function of the metal-O bond lengths in the structure. The polyhedral edge distances between nonequivalent *i*-*j* O atoms are derived from the same type of equations by geometry operations. The predictions of lattice parameters and interatomic distances from the constituent cation radii are not as accurate as those demanded by most lattice-energy calculation methods, but they are an essential step for the optimization technique that follows.

TABLE 2. Coordinate positions of O atoms as labeled in Figure 1 and equations relating structural parameters of garnets to cation radii

Equivalent O atoms	Position in the cell
O1	x, y, z
O2	$x, -y, \frac{3}{2} - z$
O3	$\frac{1}{4} - x, z - \frac{3}{4}, \frac{3}{4} - y$
O4	$\frac{1}{2} - z, -x, \frac{1}{2} + y$
O5	$z - \frac{1}{2}, x, \frac{1}{2} - y$
O6	$\frac{1}{4} + x, z - \frac{3}{4}, \frac{1}{4} + y$
O7	$\frac{3}{4} - z, \frac{1}{4} + y, \frac{3}{4} + x$
O8	$z - \frac{1}{2}, x, \frac{1}{2} - y$

Equation for O fractional coordinates

$$X_0 = 0.0258R_x + 0.0093R_y - 0.0462R_z + 0.0171$$
$$Y_0 = -0.0261R_x + 0.0261R_y - 0.0310R_z + 0.0514$$
$$Z_0 = -0.0085R_x + 0.0323R_y - 0.0237R_z + 0.6501$$

Equation for metal-O distances

$$X_1\text{-O} = 0.558R_x + 0.298R_y + 0.244R_z + 1.477$$
$$X_2\text{-O} = 0.702R_x + 0.083R_y + 1.673$$
$$Y\text{-O} = 0.154R_x + 0.754R_y + 0.132R_z + 1.316$$
$$Z\text{-O} = 1.026R_z + 1.366$$

Equation for lattice parameters

$$a_0 = 8/5\{3(X1\text{-O})^2/2 + 2(X2\text{-O})^2 + 7(Y\text{-O})^2/5 + 3(Z\text{-O})^2/2 + \{[3(X1\text{-O})^2/2 + 2(X2\text{-O})^2 + 7(Y\text{-O})^2/5 + 3(Z\text{-O})^2/2]^2 - 20[(X1\text{-O})^2 - (Z\text{-O})^2]^2 - 5[(X1\text{-O})^2 - 4(X2\text{-O})^2 + 2(Y\text{-O})^2 + (Z\text{-O})^2]^2/4 - 5[(X1\text{-O})^2 - 2(Y\text{-O})^2 + (Z\text{-O})^2]^2\}^{1/4}\}^{1/4}$$

Simulation at $P = 1$ bar, $T = 298.15$ K

The underlying principle of the method is that a structure can be determined solely by its interatomic distances when the number of nonequivalent distances in the structure is greater than the number of adjustable parameters. Therefore, if one can predict these nonequivalent distances for a given structure, then one can use these distances as "observations" in a distance least-squares refinement (DLS). The DLS procedure is an interaction technique that adjusts the positional parameters of the ions and the lattice parameters in the structure until the discrepancy between the predicted distances (observations) and the simulated ones is minimized. This method wa first developed by Meier and Villiger (1969), who found that each distance in the trial structure model must have a proper statistical weight. The inclusion of proper weights allows a satisfactory reproduction of the experimental structures. An updated version of the procedure is adopted here, DLS-76 by Baerlocher et al. (1977), which is an extension of the previous versions of Meier and Villiger (1969) and Guigas (1975). The function to be minimized is expressed by

$$R = \sum_{j=1}^{m} W_j^2 [D_{j(\text{calc})} - D_{j(\text{pred})}]^2 \quad (1)$$

where W_j is the weight assigned to the observable, $D_{j(\text{calc})}$ is the calculated distance, derived from lattice parameter and O positional parameters through symmetry operations, $D_{j(\text{pred})}$ is the predicted distance transferred to DLS from Table 2 equations, and the summations are extended over all the (m) distances in the asymmetric unit.

TABLE 3. Ionic radii of Shannon and Prewitt (1969) and Shannon (1976) compared with the garnet crystal radii and repulsive radii derived in this study

Cations	Ionic radii (Å) (Shannon and Prewitt 1969; Shannon 1976)	Garnet crystal radii (Å)	Repulsive radii (Å) at $\rho = 0.48$ Å
Mg^{2+}	0.89	0.8905	0.8833807
Fe^{2+}	0.92	0.9295	0.9362677
Mn^{2+}	0.96	0.9852	0.9693163
Ca^{2+}	1.12	1.1200	1.1363852
Al^{3+}	0.535	0.5350	0.5256711
Cr^{3+}	0.615	0.6270	0.7280560
Fe^{3+}	0.645	0.6655	0.6651070
Si^{4+}	0.26	0.2600	0.26
O^{2-}	1.40	1.4000	1.40

Note: All figures must be kept as significant to avoid rounding errors.

As mentioned above, Meier and Villiger (1969) found it necessary to assign a weighting factor to input distances in order to simulate, with sufficient accuracy, the observed values. Distances with large weight factors vary little during refinements, whereas distances with low weight factors may vary substantially. Baur (1971, 1972, 1977, 1981), therefore, proposed a weighting scheme in which the W_j factor is proportional to Pauling's bond strength (Pauling 1960) for the cation-anion distances. In this study, we assumed $W_{\text{Si-O}} = 1.0$, $W_{Y\text{-O}} = 0.5$, and $W_{X\text{-O}} = 0.25$, whereas the weight for the O-O distances was set arbitrarily at 0.07 (see Baur 1971, 1972, 1977, 1981). The weighting scheme led to a satisfactory reproduction of the grossular lattice parameter, using Shannon's (1976) ionic radii of Ca^{2+}, Al^{3+}, Si^{4+}, and O^{2-}. The ionic radii of Mg^{2+}, Fe^{2+}, Mn^{2+}, Cr^{3+}, and Fe^{3+} had to be modified slightly with respect to Shannon and Prewitt's (1969) and Shannon's (1976) values (cf. Table 3) to match the structure of pyrope (Mg^{2+}), almandine (Fe^{2+}), spessartine (Mn^{2+}), uvarovite (Cr^{3+}), and andradite (Fe^{3+}) (Table 4). We considered these modified radii to be more pertinent to the garnet structure and adopted them to derive the structures of the six uncommon garnets (Table 4, lower part).

Because the determination of the crystal radii in garnet depends upon the choice of appropriate reference structures we wish to stress that, besides the references listed in Table 1, additional data have been produced on the various natural and synthetic garnet end-members that are common. Unfortunately, consistency between data sets is poor. For example, cell-edge determinations for pyrope at room T-P conditions range from 11.452 to 11.462 Å (Haselton and Westrum 1980; Geiger et al. 1989a, 1989b; O'Neill et al. 1991; Armbruster et al. 1992; Ganguly et al. 1993); for almandine the cell-edge values range from 11.521 to 11.529 Å (Robie et al. 1967; Hsu 1968; Kawasaki and Matsui 1977; Chatillon-Colinet et al. 1983; Armbruster et al. 1992; Anovitz et al. 1993; Woodland and O'Neill 1993); for andradite proposed cell edges span 12.058–12.064 Å (Gustafson 1974; Liou 1974; Suwa et al. 1976; Robie et al. 1987; Armbruster and

TABLE 4. Structural parameters of garnets

Compounds	Lattice param.			O positional param.		
	Observed	Predicted*	Simulated**	x_0**	y_0**	z_0**
Pyrope	11.459	11.4431	11.4591	0.03291	0.05033	0.65364
Almandine	11.526	11.5143	11.5263	0.03960	0.04925	0.65330
Spessartine	11.621	11.6154	11.6210	0.03545	0.04770	0.65281
Grossular	11.845	11.8578	11.8453	0.03902	0.04399	0.65163
Uvarovite	11.996	11.9916	11.9962	0.03982	0.04664	0.65463
Andradite	12.058	12.0499	12.0583	0.04016	0.04772	0.65588
Knoringite	—	11.5806	11.6040	0.03387	0.05290	0.65676
Calderite	—	11.8105	11.8288	0.03672	0.05137	0.65715
Skiagite	—	11.7107	11.7320	0.03529	0.05288	0.65769
Khoharite	—	11.6405	11.6637	0.03427	0.05395	0.65806
Manganese chromium garnet	—	11.7514	11.7683	0.03635	0.05030	0.65588
Iron chromium garnet	—	11.6511	11.6720	0.03489	0.05183	0.65640

Note: The sources of the observed data are listed in Table 1.
* Values obtained from Basso's (1985) equation for lattice parameters (input values).
** Values obtained after DLS refinement of input data.

TABLE 5. Experimental bulk moduli of common garnet end-members

Garnets	K_0*	K_0**	Method	Ref.
Pyrope	1.90		XR	a
	1.73		US	b
	1.71–1.76		XR	c
	1.75		XR	d
	1.71–1.75		BS	e
	1.79		XR	f
	1.728		BS	q
		1.658	US	g
		1.682	US	h
		1.73	US	i
Almandine	1.68		XR	a
	1.75–1.80		XR	c
	1.76–1.68		XR	p
		1.800	XR	j
		1.801	US	g
		1.779	US	b
		1.779	US	i
		1.76–1.79	BS	e
Spessartine	1.742		US	b
		1.723	US	g
		1.74	BS	e
		1.788	BS	r
Grossular	1.75		XR	k
	1.704		US, XR	m
	1.684		BS	r
		1.705	US	g
		1.691	US	b
		1.60–1.69	**	e
Uvarovite	1.62		BS	n
		1.40–1.45	US	b
		1.34–1.68	BS	e
Andradite	1.57		BS	n
	1.59		XR	f
		1.379	US	b
		1.37–1.43	BS	e

Note: References are as follows: a = Takahashi and Liu (1970), b = Babuska et al. (1978), c = Sato et al. (1978), d = Levien et al. (1978), e = Leitner et al. (1980), f = Hazen and Finger (1989), g = Isaack and Graham (1976), h = Bonczar et al. (1977), i = Sumino and Nishizawa (1978), j = Bassett and Takahashi (1974), k = Weaver et al. (1976), m = Halleck (1973), n = Bass (1986), p = Yagi et al. (1987), q = O'Neil et al. (1991), and r = Bass (1989). Abbreviations are as follows: XR = X-ray compression method, US = ultrasonic method, and BS = Brillouin-scattering method.
* Direct measurement of end-member (synthetic or natural).
** Derived value from measurements of intermediate compound.

Geiger 1993; Woodland and Ross 1994). The crystal radii adopted here are pertinent to the selected reference structures (Table 1). The simulated structures thus bear the same range of uncertainty resulting from the comparison of values in the literature; however, full internal consistency between the simulated end-member is obtained.

Simulation at high *P*

The experimental compressibility data for the six common garnets are summarized in Table 5. The elastic properties of garnets were determined by several authors using either acoustic (ultrasonic resonance, Brillouin scattering) or static compression methods. Some of the measurements were obtained from natural samples, from which extrapolations were made by various workers to estimate the elastic properties of the end-members, as shown in Table 5. Fortunately, direct measurements were also made on each of the six common end-member or nearly end-member garnets (>95% pure, synthetic or natural end-members). For a given polyhedron in the garnet structure, the variation of metal-O bond distance with pressure is described by the linear compressibility parameter, β_1, as

$$D_P = D_{P_0}\exp[-\beta_1(P - P_0)]. \quad (2)$$

Furthermore, β_1 is linked to the zero-pressure polyhedral bulk modulus, K_0, through

$$\beta_1 = K_0^{-1}/3. \quad (3)$$

Polyhedral bulk moduli are, however, expected to vary with P. Among the existing formulations in this regard, we found that polyhedral compressibilities are best described by a modified Tait's expression, first applied by Grover et al. (1973) to simple metals:

$$K_P = K_0\frac{c + V_0/V}{c + 1}\exp\left(\frac{c\Delta V}{V_0}\right) \quad (4)$$

where c is a fitting constant.

By application of Equations 2–4, we calculated, at various P, all independent interionic distances in the asym-

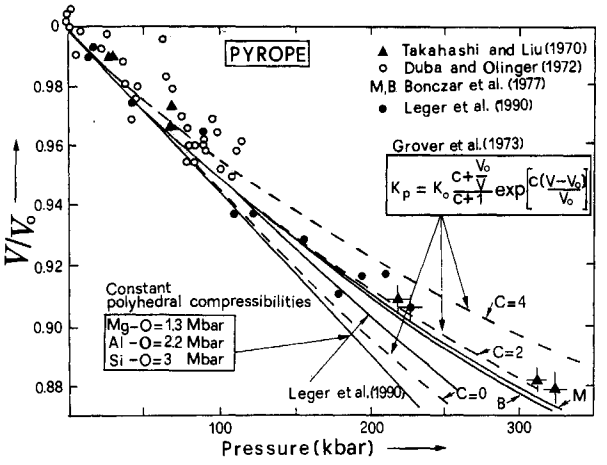

FIGURE 2. Compressional behavior of pyrope. M and B solid curves are, respectively, first-order Murnagham and first-order Birch fittings of the experimental data according to Bonczar et al. (1977). Dashed lines outline the results of structural simulation using Grover et al. (1973) equation for different values of the slope coefficient C. The results of a constant polyhedral compressibility model are also shown for comparison.

metric unit of pyrope and refined the input values by the DLS treatment. We adopted for this purpose the polyhedral bulk moduli of Hazen and Finger (1982) ($K_{0,Mg\text{-}O}$ = 1.3 Mbar; $K_{0,Al\text{-}O}$ = 2.2 Mbar; $K_{0,Si\text{-}O}$ = 3.0 Mbar). As shown in Figure 2, the compressional behavior of pyrope is reproduced within experimental uncertainties up to more than 300 kbar by choosing the value of 2.0 for the adjustable c parameter.

On the basis of the observations of Grover et al. (1973) for simple metals, we assumed the slope coefficient, c, to be constant for all isostructural compounds. Moreover, because polyhedral bulk moduli were available for only Si-O (tetrahedron), Al-O (octahedron), and Mg-O, Ca-O (dodecahedron), we calculated the remaining polyhedral bulk moduli of interest through an empirical relationship relating polyhedral compressibilities to the charge of the cation at the center of polyhedron Z_c, to the charge of ligand (Z_a), and to its metal-ligand bond distances ($D_{c\text{-}a}$) (Hazen and Prewitt 1977; Hazen and Finger 1979, 1982):

$$K_0 = 7.5(\pm 0.2)\frac{Z_c Z_a S_i^2}{D_{c-a}^3} \quad (5)$$

where S_i^2 is an empirical term for the relative ionicity of the bond (S_i^2 = 0.5 for oxides and silicates). The bulk modulus and its first and second derivative were calculated with the use of the EOS listed in Table 6 and the P-V relations obtained for various compounds.

Table 7 summarizes the results of our calculations relative to the compression of garnet and includes the six uncommon garnets for which experimental data are scanty or lacking. The results of calculations for common garnet components are consistent with experimental indications, although the calculated bulk moduli of uvarovite and andradite are somewhat higher than the literature values (cf. Tables 7 and 5). Figure 3 shows how first-order Birch-equation model parameters conform to the high-P experimental data of Leger et al. (1990) for uvarovite. According to Leger et al. (1990), experimental compression studies on garnets at high-P conditions are affected by anisotropic stress effects in solid pressure-transmitting media (<0.9% of relative volume difference). On the basis of their experimental results and assuming a bulk modulus K_0 of 1.65 Mbar, Leger et al. (1990) indicated a pressure derivative of 4.7 ± 0.7 for uvarovite. As shown in Figure 3 our model calculations conform rather well to the uncorrected experimental observations, whereas the compressional behavior suggested by Leger et al. (1990) to account for anisotropic stress (dashed line in Fig. 3) implies a volume that is more markedly P dependent. In any case, given that anisotropic stress effects are undetectable at <100 kbar, our calculated bulk modulus is consistent with the experimental results in the low-P region.

Simulation at high T

The mean linear polyhedral thermal expansion in the T range 20–1000 °C ($\bar{\alpha}_{1000}$) in O-based polyhedra is related to the charge of the central cation and the coordination number (n) through the empirical equation (Hazen and Prewitt 1977)

$$\bar{\alpha}_{1000} = 32.9\left(0.75 - \frac{Z_c}{n}\right) \times 10^{-6}(°C^{-1}). \quad (6)$$

Metal-to-O bond distances may be described at various T by

$$D_T = D_{T_0}\exp[-\alpha_1(T - T_0)]. \quad (7)$$

Thus, we may derive from Equations 6 and 7 and by

TABLE 6. Equations of state adopted in compressibility calculations

Equation	Acronym	Form
First-order Birch	BE1	$Z = \frac{3}{2}(X^{7/3} - X^{5/3})[1 + \frac{3}{4}(\eta - 4)(X^{2/3} - 1)]$
Second-order Birch	BE2	$Z = \frac{3}{2}(X^{7/3} - X^{5/3})\{1 + \frac{3}{4}(\eta - 4)(X^{2/3} - 1) + \frac{1}{24}[143 + 9\eta(\eta - 7) + 9\phi](X^{2/3} - 1)^2\}$
First-order Munaghan	ME1	$Z = \eta^{-1}(X^{\eta} - 1)$
Second-order Munaghan	ME2	$Z = [2X^{(\eta^2 - 2\phi)^{1/2}} - 1]/\{(\eta^2 - 2\phi)^{1/2}[X^{(\eta^2 - 2\phi)^{1/2}} + 1] - \eta[X^{(\eta^2 - 2\phi)^{1/2}} - 1]\}$, $(\eta^2 \geq 2\phi)$
Keane	KE	$Z = [\eta^3/(\eta^2 + \phi)^2][X^{(\eta^2 + \phi)/\eta} - 1] - [\phi/(\eta^2 + \phi)]\ln X$, $(-\eta^2 < \phi < 0)$
Born Mie	BME	$Z = 3[X^{(\eta + 3)/3} - X^{4/3}]/(\eta - 1)$
Born Mayer	BMYE	$Z = 3\{X^{2/3}\exp[(-r^0/\rho)(X^{-1/3} - 1)] - X^{4/3}\}[(r_0/\rho) - 2]^{-2}$

Note: $Z = (P - P_0)/K_0$, $\eta = K_0'$, $\phi = K_0K_0''$, and $X = V_0/V$.

TABLE 7. Isothermal bulk modulus and its pressure derivative for garnet end-members in the range $P = 0$–300 kbar (25 °C) obtained with the fictive compression model

Compound	K_0	K'_0	K''_0	$\chi^2 \times 10^4$
		Pyrope		
BE1	1.77604	4.78350		1.30
ME1	1.78085	4.56623		2.50
BE2	1.78023	4.60247	−0.59978	2.30
ME2	1.77947	4.62373	−0.59993	2.00
KE	1.76854	4.59606		2.50
BME	1.77672	7.25925		1.40
BMYE	1.77563	9.67061		1.10
		Almandine		
BE1	1.83655	4.79524		1.20
ME1	1.84130	4.58191		2.30
BE2	1.84050	4.61990	−0.59900	2.10
ME2	1.83990	4.63960	−0.60000	1.90
KE	1.83670	4.59140		2.30
BME	1.83726	7.29469		1.30
BMYE	1.83610	9.70365		1.10
		Spessartine		
BE1	1.79731	4.83288		2.40
ME1	1.80222	4.61226		3.90
BE2	1.80143	4.64989	−0.59900	3.60
ME2	1.80085	4.66941	−0.60000	3.30
KE	1.79181	4.63689		3.90
BME	1.79805	7.40000		2.60
BMYE	1.79693	9.80764		2.30
		Grossular		
BE1	1.67284	4.88739		1.40
ME1	1.67801	4.65022		2.90
BE2	1.67729	4.68640	−0.60000	2.60
ME2	1.67667	4.70722	−0.60000	2.40
KE	1.66667	4.68011		2.90
BME	1.67370	7.54733		1.60
BMYE	1.67249	9.96224		1.30
		Uvarovite		
BE1	1.74317	4.97674		3.40
ME1	1.74851	4.73545		5.50
BE2	1.74775	4.77285	−0.59900	5.10
ME2	1.74717	4.79261	−0.60000	4.80
KE	1.74852	4.73515		5.50
BME	1.74421	7.79868		3.70
BMYE	1.74299	10.20348		3.30
		Andradite		
BE1	1.72559	4.90995		2.20
ME1	1.73080	4.67448		4.00
BE2	1.73013	4.70962	−0.59900	3.70
ME2	1.73385	4.66248	−0.50272	5.20
KE	1.73079	4.67448		4.00
BME	1.72646	7.61347		2.50
BMYE	1.72532	10.02130		2.10
		Knoringite		
BE1	1.87573	4.84250		1.80
ME1	1.88054	4.62767		3.20
BE2	1.87991	4.64967	−0.24550	3.10
ME2	1.87916	4.68521	−0.59900	2.70
KE	1.86501	4.66300		3.20
BME	1.87642	7.43236		2.00
BMYE	1.87527	9.83566		1.70
		Calderite		
BE1	1.81769	4.82315		2.00
ME1	1.82253	4.60545		3.40
BE2	1.82041	4.66029	−0.59798	3.20
ME2	1.82117	4.66285	−0.59944	2.90
KE	1.80965	4.63582		3.40
BME	1.81841	7.37421		2.20
BMYE	1.81734	9.77909		1.90
		Skiagite		
BE1	1.86692	4.76181		0.56
ME1	1.87152	4.55478		1.40
BE2	1.87071	4.59268	−0.59712	1.20
ME2	1.87012	4.61253	−0.59998	1.00
KE	1.85412	4.59587		1.40
BME	1.86756	7.20140		0.65
BMYE	1.86644	9.60920		0.49
		Khoharite		
BE1	1.85660	4.79862		2.70
ME1	1.86086	4.59516		4.10
BE2	1.86006	4.63345	−0.59987	3.80
ME2	1.85951	4.65237	−0.60000	3.60
KE	1.84557	4.63252		4.10
BME	1.85680	7.33299		2.90
BMYE	1.85575	9.73702		2.60
		Manganese chromium garnet		
BE1	1.85174	4.89417		3.00
ME1	1.85671	4.67195		4.60
BE2	1.85613	4.70559	−0.59560	4.30
ME2	1.85087	4.77763	−0.50776	7.40
KE	1.84455	4.70400		4.70
BME	1.85258	7.57399		3.30
BMYE	1.85148	9.97493		2.90
		Iron chromium garnet		
BE1	1.90211	4.83062		1.50
ME1	1.90682	4.61968		2.60
BE2	1.90509	4.66410	−0.59987	6.70
ME2	1.90548	4.67659	−0.59951	2.20
KE	1.89083	4.65793		2.60
BME	1.90281	7.40000		1.60
BMYE	1.90176	9.79821		1.40

Note: Acronyms are defined in Table 6. Precisions are reported as χ^2 summation over 31 P values (step = 10 kbar).

application of trigonometric rules and DLS treatment, the mean thermal expansion of the phase in the T range of interest, in a fashion analogous to that already seen for the P effect on the structure. Equation 6 furnishes, however, only a rough estimate of mean linear thermal expansion in a restricted T range, and we know from experiments that thermal expansion is a nonlinear function of T. Concerning garnets, the existing thermal expansion data represent a T dependence of the type (Skinner 1956)

$$\alpha_{V,T} = \frac{1}{V}\left(\frac{\partial V}{\partial T}\right)_P = \alpha_0 + \alpha_1 T + \alpha_2 T^{-2}. \quad (8)$$

We therefore assumed that linear thermal expansion coefficients for the various polyhedra obey a T dependence of this type and assigned to the different cations in the different coordination states α_0 values consistent with Equation 6 and with values in the literature (see Hazen and Finger 1982; Table 6–3). Initial estimates were then adjusted with a trial-and-error procedure until satisfactory reproduction of experimental data was achieved.

Results of the calculations are listed in Table 8. As illustrated in Figure 4, the thermal expansion coefficients derived in this work for common garnets agree with the experimental data within the limits of experimental uncertainties (which are rather large, especially at low T; see Skinner 1956). In the case of pyrope, calculated low-T thermal expansion coefficients are more consistent with

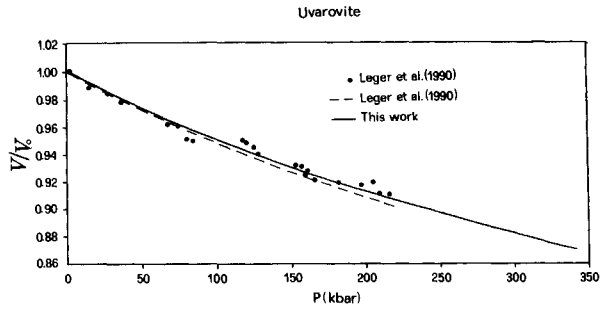

FIGURE 3. Compressional behavior of uvarovite. The solid curve is the first-order Birch EOS calculated in this study (see Table 10).

the experimental observations of Suzuki and Anderson (1983) and approach the values of Skinner (1956) at higher T. Calculated thermal expansion values for grossular are more consistent with the data of Isaak et al. (1992) than with the results of Skinner (1956), especially in the low T (25–100 °C) and high T (1100–1400 °C) ranges. Calculated low-T thermal expansions for andradite are consistent with the experiments of Armbruster and Geiger (1993) and agree with the experimental observations of Skinner (1956) at high T. For spessartine and almandine, the reproduction of the data of Skinner (1956) is rather satisfactory, disregarding the somewhat higher values obtained in the low-T range. Concerning the numerical solution, as already noted, α_0 terms of polyhedral linear thermal expansion are consistent with tabulated values (Hazen and Finger 1982). In particular, the α_0 value obtained for $^{[8]}Mg^{2+}$ is identical to the mean linear thermal expansion term observed by Meagher (1975) in pyrope; the α_0 values obtained for $^{[8]}Ca^{2+}$, $^{[6]}Fe^{3+}$, $^{[6]}Al^{3+}$, and $^{[6]}Cr^{3+}$ are close to the tabulated low limit of the mean linear thermal expansion values of Hazen and Finger (1982). Values of α_1 and α_2 were unique for all cations in all coordination states, corresponding to 1.0×10^{-9} and -0.1, respectively.

TABLE 8. Volume thermal expansion coefficients for common and uncommon compositional terms of garnets compared with experimental regressions

Compound	$\alpha_0 \times 10^5 K^{-1}$	$\alpha_1 \times 10^9 K^{-2}$	$\alpha_2 K$	Ref.
Pyrope	2.431	5.649	−0.2205	1
	2.311	5.956	−0.4538	2
	2.244	9.264	−0.1761	3
Almandine	1.781	11.558	−0.2000	1
	1.776	12.140	−0.5071	2
Spessartine	2.962	2.398	−0.8122	1
	2.927	2.726	−1.1560	2
Grossular	2.224	5.272	−0.4119	1
	1.951	8.089	−0.4972	2
	2.610	3.390	−0.7185	4
Uvarovite	2.232	5.761	−0.2329	1
Andradite	2.208	6.019	−0.2005	1
	2.103	6.839	−0.2245	2
	1.869	9.909	−0.1486	5
Knoringite	2.894	2.9642	−0.7748	1
Calderite	2.898	3.7316	−0.5455	1
Skiagite	2.336	7.0286	−0.2950	1
Khoharite	2.626	5.3687	−0.4521	1
Manganese chromium garnet	2.862	4.0015	−0.5160	1
Iron chromium garnet	2.584	3.7865	−0.4282	1
$^{[8]}Mg^{2+}$	1.300	1.0	−0.1	
$^{[8]}Fe^{2+}$	1.200	1.0	−0.1	
$^{[8]}Mn^{2+}$	1.400	1.0	−0.1	
$^{[8]}Ca^{2+}$	1.100	1.0	−0.1	
$^{[6]}Al^{3+}$	0.700	1.0	−0.1	
$^{[6]}Cr^{3+}$	0.800	1.0	−0.1	
$^{[6]}Fe^{3+}$	0.800	1.0	−0.1	
$^{[4]}Si^{4+}$	0.200	1.0	−0.1	

Note: Volume thermal expansion polynomia for andradite, pyrope, and grossular were obtained from Armbruster and Geiger (1993), Suzuki and Anderson (1983), and Isaak et al. (1992), respectively, by a nonlinear minimization procedure on the reported experimental observations. References are as follows: 1 = this work, 2 = Skinner (1956), 3 = Suzuki and Anderson (1983), 4 = Isaak et al. (1992), 5 = Armbruster and Geiger (1993). In the lower part of the table are listed the adopted polyhedral linear thermal expansion coefficients.

STATIC ENERGY AND ENTHALPY

The lattice energy of a solid at a given P-T condition can be considered, in the static approximation, as composed of coulombic (E_c), repulsive (E_r), dispersive (E_{dd}, E_{dq}), and crystal-field stabilization terms (E_{cfs}) resulting from the sum of pair interactions among all ions in the crystal:

$$U_{P,T} = E_{c,P,T} + E_{r,P,T} + E_{dd,P,T} + E_{dq,P,T} + E_{cfs,P,T}$$
$$= \sum_{i=1}^{n}\sum_{j=i}^{n} Z_i Z_j C_{ij}^{c} + \sum_{i=1}^{n}\sum_{j=i}^{n} b_{ij} C_{ij}^{r}$$
$$+ \sum_{i=1}^{n}\sum_{j=i}^{n} dd_{ij} C_{ij}^{dd} + \sum_{i=1}^{n}\sum_{j=i}^{n} dq_{ij} C_{ij}^{dq}$$
$$+ \sum_{i=1}^{n'} cfs_{il} C_{il}^{cfs}. \quad (9)$$

The double summations in Equation 9 comprise all the n ions in the asymmetric unit, whereas the last term is limited to first neighbors (n') in a cation-to-ligand (l) field. The structural factors C_{ij}^{c}, C_{ij}^{r}, C_{ij}^{dd}, C_{ij}^{dq}, and C_{il}^{cfs} reflect the dependency of the various static potentials over the interionic distance; they are geometrically related to cell edges and atom positional parameters and can be evaluated with the aid of rapidly converging automated routines performing direct summation (to account for partial charge overlap) and Ewald's summation over the reciprocal space (Catti 1978, 1981). Expanding the coefficients of the various forms of energy along the guidelines outlined in previous publications (Ottonello 1987, 1992; Ottonello et al. 1990, 1992; Della Giusta and Ottonello 1993) and accounting for the fact that the lattice energy of a substance at the P_r,T_r reference condition must obey the energy balance imposed by the Born-Haber-Fayans thermochemical cycle, one obtains

$$\sum_{i=1}^{n}\sum_{j=i}^{n} \beta_{ij} b \exp\left(\frac{r_i + r_j}{\rho}\right) C_{ij}^{r}$$
$$= \sum_{i=1}^{m} E_{s,m} + 6E_{D,O_2} + 12E_{A,O}$$

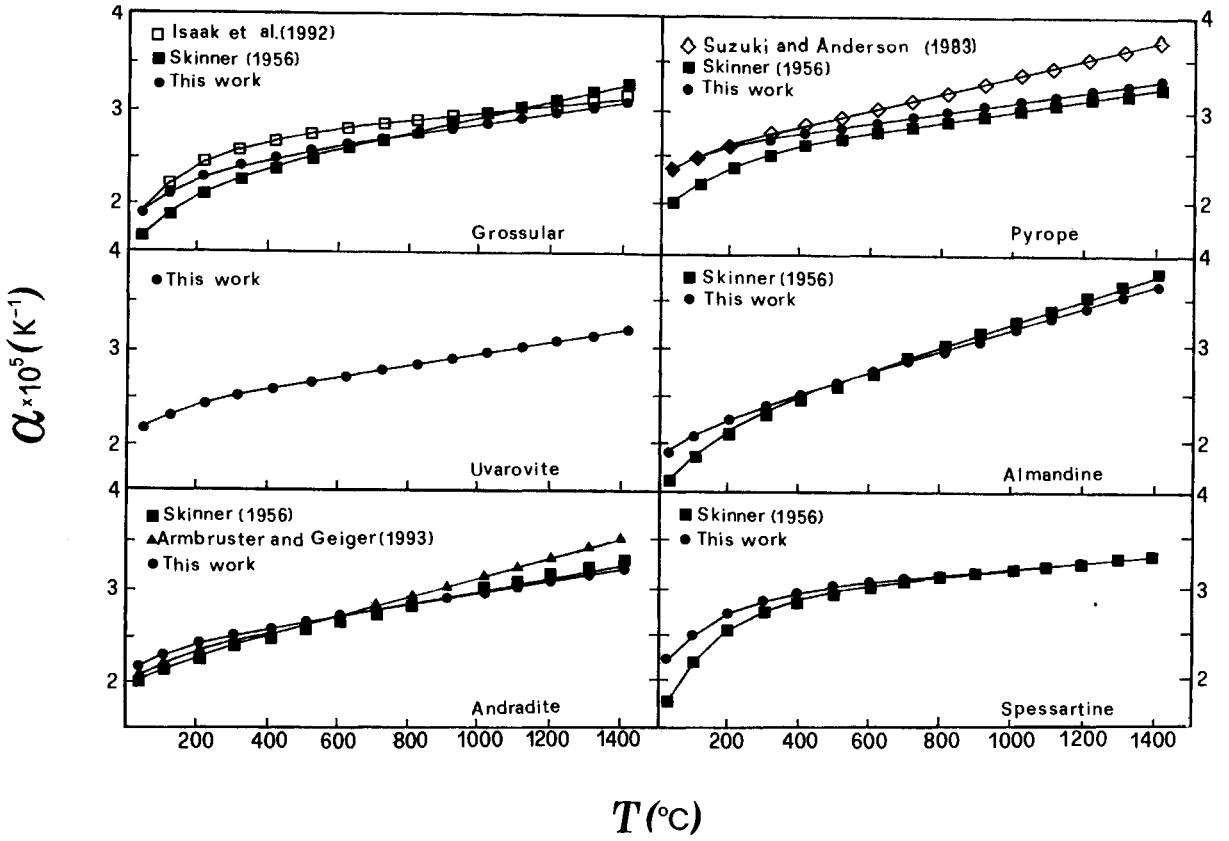

FIGURE 4. Isobaric thermal expansion of the common garnet end-members by structural simulation in comparison with the experimental data. The various thermal expansion coefficients are listed in Table 11.

$$+ \sum_{i=1}^{m} \sum_{v} E_{I,m} - H^{0}_{f,P_r,T_r}$$

$$- \sum_{i=1}^{n} \sum_{j=i}^{n} Z_i Z_j C^{c}_{ij}$$

$$- \sum_{i=1}^{n} \sum_{j=i}^{n} \frac{3}{2} \alpha_i \alpha_j \frac{\bar{E}_i \bar{E}_j}{(\bar{E}_i + \bar{E}_j)} C^{dd}_{ij}$$

$$- \sum_{i=1}^{n} \sum_{j=i}^{n} \frac{27}{8} \frac{\alpha_i \alpha_j}{e^2 (\bar{E}_i + \bar{E}_j)} \left(\frac{\alpha_i \bar{E}_i}{n_{e,i}} + \frac{\alpha_j \bar{E}_j}{n_{e,j}} \right) C^{dq}_{ij}$$

$$- \sum_{i=1}^{n'} \left(\frac{2}{5} \frac{Z_{e,l} a_i^4}{\bar{D}_{il}^5} + \frac{\delta_i + \sigma_i}{3} \right) - 20RT_r \qquad (10)$$

where b = repulsive factor of the substance; r_i, r_j = repulsive radii of the i and j ions, respectively; ρ = hardness factor of the family of compounds; $E_{S,m}$ = sublimation energy of the metal m; E_{D,O_2} = dissociation energy of molecular O_2; $E_{A,O}$ = electron affinity of atomic O; $E_{I,m}$ = ionization energy of the metal m; H^0_{f,T_r,P_r} = enthalpy of formation from the elements at reference conditions; Z_i, Z_j = formal ionic charges for i and j ions, respectively; α_i, α_j = free ion polarizabilities; $\bar{E}_i$, $\bar{E}_j$ = mean excitation energies; $n_{e,i}$, $n_{e,j}$ = effective electrons; e = electronic charge; $Z_{e,l}$ = effective charge of the ligand; a_i = mean of the radial distance for the d electrons of the ith cation; D_{il} = metal-to-ligand interionic distance; δ_i = maximum splitting of t_{2g} orbital levels for the ith cation; σ_i = energy splitting between the two lowest t_{2g} for the ith cation; and R = gas constant.

TABLE 9. Magnitudes involved in the Born-Haber-Fajans cycle of end-member garnets

	Mg^{2+}	Fe^{2+}	Ca^{2+}	Mn^{2+}	Cr^{3+}	Al^{3+}	Fe^{3+}	Si^{4+}	O^{2-}
Polarizability (Å)	0.069	0.6875	0.511	0.499	0.33	0.0419	0.234	0.0255	1.694
Excitation (eV)	58.65	22.98	38.41	25.27	38.25	89.97	42.00	125.05	19.90
Outer electrons	8	6	6	5	3	8	5	8	8
Polarizable electrons	2.123	3.247	6.742	2.849	2.617	3.033	3.905	3.566	6.000
Effective electrons	4.121	4.414	7.344	3.775	2.802	4.926	4.419	5.341	6.928
Ionization energy (eV)	22.67	24.08	17.98	23.07	54.25	53.24	54.72	103.08	
Sublimation energy (eV)	1.52	4.33	1.83	3.04	4.10	3.25	4.33	4.56	

All the variables on the right side of Equation 10 are experimentally known (Table 9), as are the structural coefficients of the static potentials after an appropriate structural simulation and DLS treatment, as previously discussed. Equation 10 then allows a parameterization of the coefficients of the repulsive (short-range) potential in the chemical space of interest. The enthalpy values are available only for the common end-members (see Table 10). Nevertheless, these end-members contain all the types of atoms present in the system. Static energy calculations for the six common garnet end-members were then made using the various values of the hardness factor, ρ, at T_r, P_r reference conditions, assuming repulsive radii to coincide with the mean crystal radii in the structure. This choice is consistent with the concept of effective distribution radius (EDR) as defined by the limit of lowest electron density between neighboring ions and with the quantum-mechanical short-range potential for closed-shell atoms (Zener 1931). Table 11 lists the static energy terms consistent with the adopted values of $\overline{H}^0_{f,T_r,P_r}$, which in most cases correspond to calorimetric estimates. For this purpose, we note that serious discrepancies become apparent in the comparison of all the proposed values in the literature for a single component (1σ = 52.1 kJ/mol for pyrope, 23.9 kJ/mol for almandine, 23.3 kJ/mol for spessartine, 31.2 kJ/mol for grossular, and 11.0 kJ/mol for andradite). These high 1σ values correspond to about 8% of $\overline{H}^0_{f,T_r,P_r}$ in the worst case and are ascribable to the high degree of eutaxy of the phase, which makes short-range disorder and intrinsic defects crucial in determining its static energy (Ottonello et al. in preparation). As shown in Table 12 and in Figure 5, repulsive energies of the various compositional terms may be parameterized under various hardness conditions. Nevertheless, only a specific b-ρ couple is appropriate in describing the increase of static energy owing to compression. For each end-member, the static lattice energy was then determined under various compression states with the b-ρ couples determined at T_r, P_r reference condition, and the appropriate hardness factor was selected by application of the equality

$$U_{P,T_r} = U_{0(P_r,T_r)} - \int_{V_0}^{V} P\,dV. \qquad (11)$$

Results of the calculations are listed in Tables 13 and 14.[1] As we see in Figure 6, the increase of static energy with pressure is quite sensitive to the hardness factor ρ. Moreover, a constant value of ρ is appropriate only within a restricted P range and, for all end-member phases, ρ increases monotonically with increasing P. The adopted (empirical) functional form of short-range repulsive potentials thus requires a hardness factor that is itself a function of P, a fact that has never been pointed out hitherto to our knowledge, because of the limited P range investigated either experimentally or computationally.

We assumed then, that the short-range static energy of the common garnets is consistent with a simple Huggins-Mayer formulation (ρ constant within a family of salts and preexponential factor b variable from salt to salt in the isostructural family of compounds) and derived the appropriate preexponential factors consistent with the operative assumption of repulsive radii coincident with

TABLE 10. Enthalpy of formation from the elements at T_r = 298.15 K, P_r = 1 bar, for common garnet end-members

Compound	$-\overline{H}^0_{T_r,P_r}$ (kJ/mol)	Reference
Pyrope	6368.41	Karpov and Kashik (1968)
	6290.76*	Charlu et al. (1975)
	6283.32	Holland and Powell (1990)
	6270.71	Ostrovskii (1990)
	6224.12	Kiseleva (1976)
Mean	6287.46	
s.d.	52.1	
Almandine	5334.31	Viellard (1982)
	5328.58	Zen (1973)
	5322.83	Fed'kin (1970)
	5319.0	Yakovlev and Vozianova (1983)
	5310.0	Bhattacharya (1986)
	5305.281	Karpov et al. (1976)
	5303.61	Karpov and Kashik (1968)
	5301.8	Karpov et al. (1971)
	5301.51	Ostrovskii (1990)
	5280.0	Karpov et al. (1977)
	5275.47	Chatillon-Colinet et al. (1983)
	5275.	Chatterjee (1987)
	5272.0	Harlow and Newton (1992)
	5267.85	Holland and Powell (1990)
	5267.8	Woodland and Wood (1989)
	5267.216	Berman (1990)
	5265.5	Berman (1988)
	5261.3*	Anovitz et al. (1993)
Mean	5292.17	
s.d.	23.9	
Spessartine	5686.934*	Boeglin (1981)
	5686.66	Karpov and Kashik (1968)
	5646.454	Viellard (1982)
Mean	5673.34	
s.d.	23.3	
Grossular	6657.12	Ostrovskii (1990)
	6656.7	Robie et al. (1978)
	6643.36	Barin et al. (1977)
	6638.3	Holland and Powell (1990)
	6632.76*	Charlu et al. (1978)
	6573.21	Karpov and Kashik (1968)
Mean	6633.57	
s.d.	31.1	
Uvarovite	6034.58*	Kiseleva (1977)
Andradite	5778.125	Helgeson et al. (1978)
	5769.7	Zhang and Saxena (1991)
	5769.36	Ostrovskii (1990)
	5763.376	Taylor and Liou (1978)
	5761.6	Holland and Powell (1990)
	5758.85*	Robie et al. (1987)
	5747.01	Kiseleva et al. (1972)
	5746.63	Viellard (1982)
Mean	5761.8	
s.d.	11.0	

Note: s.d. = standard deviation.
* Adopted values in the parameterization of short-range repulsive energy terms.

[1] A copy of Tables 13 and 14 may be ordered as Document AM-96-610 from the Business Office, Mineralogical Society of America, 1015 Eighteenth Street, Suite 601, Washington, DC 20036, U.S.A. Please remit $5.00 in advance for the microfiche.

TABLE 11. Static energy terms for the 12 garnet end-members in the system

Compound	E_{bhf}	$\overline{H}^{\circ}_{f,T_r,P_r}$	U	E_c	E_r	E_{dd}	E_{dq}	E_{cfs}
1	59269.2	−6290.8	−65560.0	−77060.6	12287.8	−599.8	−187.4	0.0
2	60487.6	−5261.3	−65749.0	−76916.7	12328.7	−769.6	−253.4	−138.0
3	59822.8	−5686.9	−65509.8	−76704.9	12097.9	−684.2	−218.6	0.0
4	57997.4	−6632.8	−64630.2	−76148.6	12360.9	−645.3	−197.2	0.0
5	58356.4	−6034.6	−64391.0	−75446.1	12396.7	−660.6	−209.1	−472.0
6	58489.9	−5758.9	−64248.8	−75160.5	11779.0	−660.5	−206.8	0.0
7	59628.2	−5576.1	−65204.4	−76294.3	12390.4	−623.9	−204.5	−472.0
8	60315.3	−4719.8	−65035.1	−75661.1	11556.8	−701.7	−229.1	0.0
9	60980.1	−4276.2	−65256.4	−75856.7	11783.8	−783.5	−262.0	−138.0
10	59761.7	−5299.5	−65061.2	−75981.6	11750.0	−626.5	−203.1	0.0
11	60181.8	−5007.1	−65188.9	−75965.8	12182.0	−701.5	−231.7	−472.0
12	60846.7	−4555.3	−65402.0	−76162.5	12420.4	−784.6	−265.3	−610.0

Note: The lattice energy is consistent with the adopted values of H°_{f,T_r,P_r} for common garnets (compounds 1–6) through Born-Haber-Fayans calculations (E_{bhf}). E_{bhf} terms are consistent with an estimated electron affinity for O of −720 kJ/mol (Greenwood 1970). Lattice energy and enthalpy of uncommon end-members were derived from single-ion repulsive factors in the framework of the Huggins-Mayer approach at ρ = 0.48 Å. Crystal-field stabilization energy contributions were maintained constant for the various transition ions because of the contrasting evidences concerning fifth-order dependency of the cation-to-ligand distance. All listed energy terms are in kilojoules per mole. Reference numbers are in Table 1.

the crystal radii in the structure. The resulting preexponential factors for the six salts in the garnet family were in the neighborhood of two and not dissimilar from each other [$\bar{b}$ = 2.017 (±0.045 × 10^{-19} J/mol); see Table 12]. When one adopts the Huggins-Mayer approach, the preexponential factor for each salt in the family of compounds reduces to an arbitrary constant, as discussed by Tosi (1964) and Tosi and Fumi (1964) (see Eq. 5.10 in Tosi 1964). Hence, we adopted for the six common end-members a common b factor corresponding to the average of the values valid for the various salts in the Huggins-Mayer generalization. We forced, in this way, the common garnet end-members to obey an ideal condition as far as the repulsive energy is concerned, i.e., a common b and common ρ factor in the family of salts (or, in other terms, a combined Huggins-Mayer, Born-Mayer approach) and derived the repulsive radii appropriate to such an ideal condition (Table 3). The energetic significance of this simplification is displayed in Figure 7: The b factor in the Huggins-Mayer approach may be considered as a dispersion of the intercept values in a logarithmic plot of first-neighbor repulsive energies vs. interionic first-neighbor distance. Because the static energies of the 12 garnet end-members are rigorously coplanar in the chemical space of interest, the enthalpy of formation from the elements, at reference conditions, is readily derived by application of Equation 9, all coefficients of the short-range interaction being parameterized by the six common compositional terms.

We wish to emphasize that to our knowledge there is no other way, besides detailed quantum-mechanical calculations, to estimate the enthalpy of formation of garnets from first principles because, being the phase near eutaxy, first-neighbor interionic energies are extremely variable from salt to salt in the family of isostructural compounds (see Table 15). This extreme sensitivity of

TABLE 12. The b-ρ couples consistent with the derived values of E_r (Huggins-Mayer generalization, see also Table 11)

Compound	ρ 0.45	0.46	0.47	0.48	0.49	0.50	0.51
1	2.0096	2.0024	1.9944	1.9856	1.9761	1.9659	1.9551
2	2.0267	2.0193	2.0111	2.0022	1.9926	1.9823	1.9714
3	1.9979	1.9907	1.9827	1.9740	1.9645	1.9544	1.9437
4	2.0407	2.0341	2.0267	2.0184	2.0095	1.9998	1.9895
5	2.1279	2.1196	2.1106	2.1008	2.0903	2.0792	2.0675
6	2.0509	2.0425	2.0333	2.0235	2.0131	2.0021	1.9905
Mean	2.0422	2.0347	2.0264	2.0174	2.0076	1.9972	1.9862
s.d.	0.0462	0.0457	0.0453	0.0449	0.0446	0.0442	0.0438

Note: Reference numbers as in Table 1; b is in J × 10^{19} and ρ is in angstroms; s.d. = standard deviation.

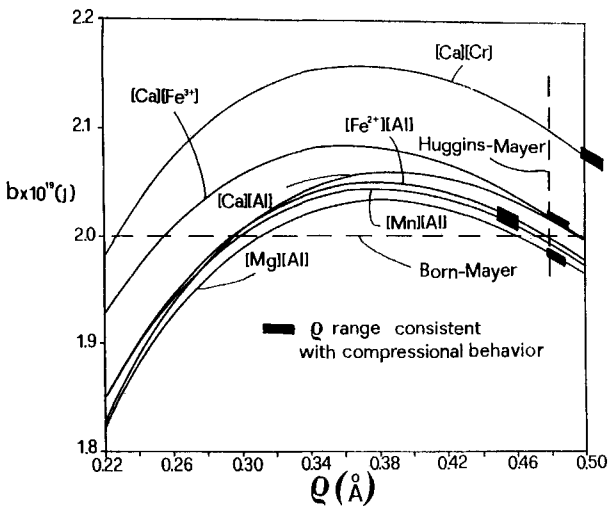

FIGURE 5. Relationship between preexponential repulsive factor b and hardness factor ρ for common garnet end-members. The horizontal and vertical dashed lines mark the point of complete ideality (in terms of the Born model), which may be attained by an appropriate selection of repulsive radii.

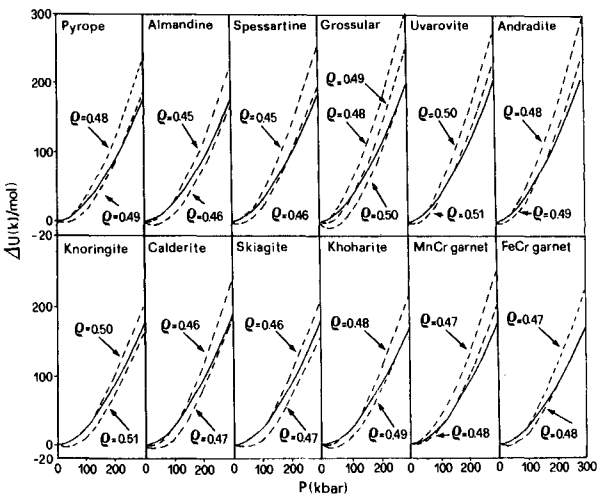

FIGURE 6. Increase of the static energy of garnet end-members with pressure, on the basis of the interionic potential model for different values of the hardness factor ρ and comparison with EOS calculations (solid lines).

interionic potentials to an atom's positional parameters also has profound consequences for the precision of the calculated interaction parameters in mixture.

HEAT CAPACITY AND ENTROPY

It is fairly well established from several studies that garnets have 25 Raman active modes ($3A_{1g}$, 8 E_g, and 14 F_{2g}) and 17 infrared-active modes (all of the same type, F_{1u}). From studies on synthetic and natural garnets, Tarte and Deliens (1973), Moore et al. (1971), and Farmer (1974) demonstrated a correlation between bands of specific frequency and the polyhedra in the crystal structure. The interpretation of the vibrational spectra allowed the assignment of the bands in the high-frequency region (800–1000 cm^{-1}) to Si-O stretching vibrations of the SiO_4 tetrahedra; the bands in the frequency range 500–600 cm^{-1} to the deformation of the SiO_4 tetrahedra under the influence of the cation species in the neighboring octahedra; and the bands under 500 cm^{-1} to complex lattice vibrations. From the observed vibrational spectra of garnets, we derived the heat capacity at constant volume C_V and the harmonic entropy S_V according to Kieffer's model (Kieffer 1979a, 1979b, 1979c, 1980, 1982). This model considers three acoustic modes (shear modes S1 and S2, and longitudinal mode P), which are approximated by a sine function (S_{Xi} "dispersed acoustic function"; cf. Kieffer 1979c). The rest of the modes ($3s - 3$, with s = number of atoms in the primitive unit cell) are optic. In the case in which some unit of the structure can be isolated (e.g., SiO_4 tetrahedra), some of the vibrational frequencies can be represented by Einstein oscillators, with q_1, q_2, . . . as a fraction of the total modes, through the Einstein function E_{XE}. The rest of the optic modes are considered to belong to an optic continuum, between lower, ω_l, and higher, ω_u, cut-off frequencies, represented by the function K_{X_l,X_u}. This simplification of the dispersion waves allows a representation of the vibrational spectrum (frequency distributions). The resulting spectrum is regarded as the sum of the three acoustic frequencies at ω_1, ω_2, and ω_3, added to the optic frequency distributions at ω_l and ω_u, which delimit the optic continuum, and the isolated

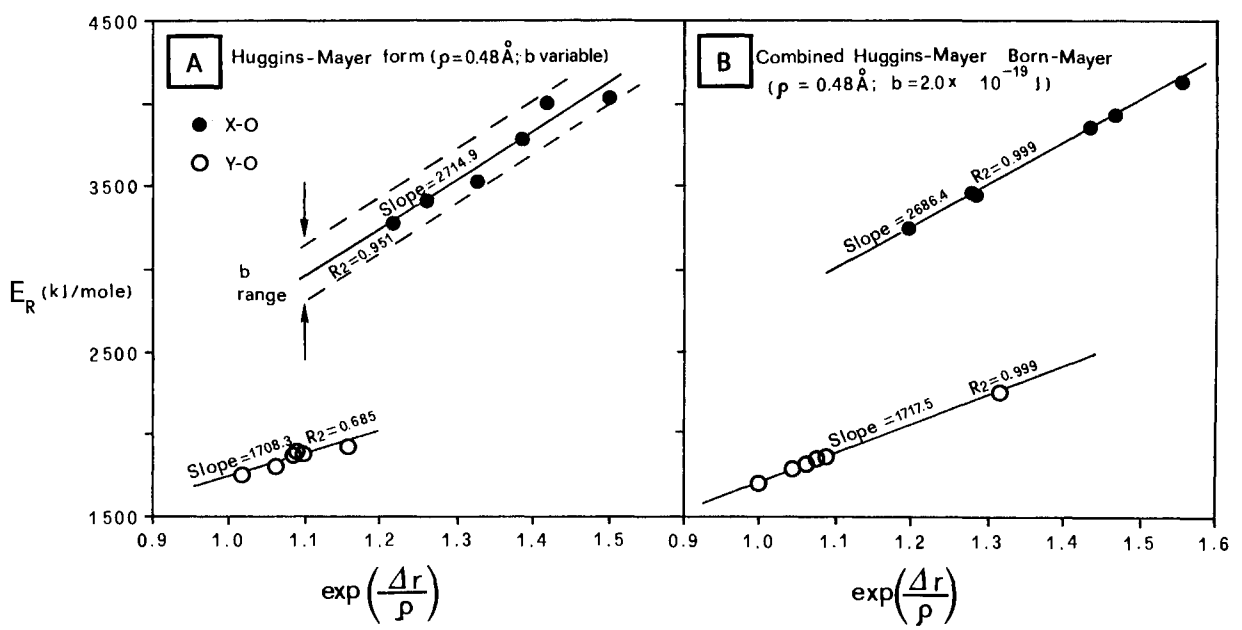

FIGURE 7. Site-repulsive energy in common garnet end-members according to the Huggins-Mayer (A) and ideal (B) formulation.

TABLE 15. First-neighbor interaction energies for the 12 garnet end-members

Ions	End-m.	E_c	E_r	E_{dd}	E_{dq}	E_{crs}	X1-O1	Y1-O4	Si-O1	O1-O2
Mg-O	1	−68252.52	3251.67	−31.73	−8.39		2.1969			
	7	−67724.96	3106.02	−30.02	−7.80		2.2240			
	10	−67523.64	3047.50	−29.34	−7.57		2.2354			
Fe^{2+}-O	2	−67756.28	3456.40	−213.90	−79.83	−138.0	2.2184			
	9	−67070.88	3238.28	−197.79	−72.09	−138.0	2.2570			
	12	−67260.88	3301.29	−202.41	−74.29	−138.0	2.2455			
Ca-O	4	−65648.96	4129.05	−147.86	−44.13		2.3247			
	5	−65295.08	3937.66	−139.98	−41.11		2.3519			
	6	−64953.72	3860.89	−136.84	−39.93		2.3634			
Mn-O	3	−67087.56	3452.29	−149.11	−52.35		2.2494			
	8	−66463.44	3232.99	−137.94	−47.31		2.2880			
	11	−66633.16	3295.49	−141.10	−48.72		2.2765			
Al-O	1	−72268.50	1857.65	−29.29	−10.96			1.8906		
	2	−72028.26	1829.85	−28.69	−10.68			1.8967		
	3	−71713.68	1791.75	−27.88	−10.29			1.9054		
	4	−71060.34	1703.28	−26.01	−9.41			1.9265		
Fe^{3+}-O	6	−68953.50	1869.35	−95.92	−39.88			2.0245		
	8	−69668.58	1968.55	−102.63	−43.45			2.0334		
	9	−69921.00	2011.46	−105.54	−45.00			1.9947		
	10	−70116.24	2042.66	−107.67	−46.15			1.9886		
Cr-O	5	−69690.72	2259.22	−81.56	−36.85	−472.0		1.9956		
	7	−70714.62	2466.96	−91.62	−42.70	−472.0		1.9596		
	11	−70234.80	2377.75	−87.28	−40.16	−472.0		1.9745		
	12	−70506.78	2429.57	−89.79	−41.63	−472.0		1.9657		
Si-O	1	−146972.48	2111.21	−45.11	−22.02				1.6327	
	2	−146729.76	2103.45	−45.02	−22.00				1.6327	
	3	−146437.84	2093.37	−44.90	−21.98				1.6328	
	4	−145961.44	2072.19	−44.64	−21.94				1.6329	
	5	−145662.72	2057.11	−44.48	−21.92				1.6328	
	6	−145159.84	2051.78	−44.43	−21.93				1.6327	
	7	−146384.40	2093.33	−44.91	−21.99				1.6327	
	8	−145819.52	2070.53	−44.64	−21.95				1.6327	
	9	−146018.64	2080.23	−44.77	−21.98				1.6327	
	10	−146182.40	2086.58	−44.83	−21.97				1.6327	
	11	−145975.36	2077.15	−44.72	−21.97				1.6327	
	12	−146195.04	2086.35	−44.83	−21.98				1.6327	
O-O	1	112409.12	4904.10	−493.30	−146.04					2.4916
	2	111981.68	4762.62	−478.76	−140.52					2.5016
	3	111446.12	4580.74	−460.24	−133.75					2.5164
	4	110473.68	4220.98	−424.10	−121.48					2.5528
	5	109690.44	3883.50	−390.74	−108.83					2.5470
	6	109002.44	3762.48	−379.01	−104.67					2.5450
	7	111350.80	4537.63	−456.66	−131.95					2.4879
	8	110175.44	4102.29	−412.99	−116.07					2.5103
	9	110616.84	4274.07	−430.36	−122.33					2.4963
	10	110973.12	4406.04	−443.81	−127.34					2.4867
	11	110505.04	4228.76	−425.29	−120.45					2.5118
	12	110973.96	4403.18	−442.94	−126.82					2.4976

Note: Energies are in kilojoules per mole. Closest-approach distances (in angstroms) are also listed. Reference numbers as in Table 1.

Einstein oscillators at ω_{E_1} and ω_{E_2}. In this representation the heat capacity at constant V is given by

$$C_V = \frac{3R}{Z}\sum_{i=1}^{3} S_{X_i} + 3nR\left(1 - \frac{1}{N} - q\right)K_{X_l,X_u} + 3nRqE_{X_E} \tag{12}$$

where

$$S_{X_i} = \left(\frac{2}{\pi}\right)^3 \int_0^{X_i} \frac{[\arcsin(X/X_i)]^2 X^2 e^2\, dX}{(X_i^2 - X^2)^{1/2}(e^X - 1)^2} \tag{13}$$

$$\mathcal{K}_{X_l,X_u} = \int_{X_l}^{X} \frac{X^2 e^X\, dX}{(X_u - X_l)^X (e - 1)^2} \tag{14}$$

$$E_{X_E} = \frac{X_E^2 e^{X_E}}{(e^{X_E} - 1)^2} \tag{15}$$

with

$$X = \frac{\hbar\omega}{kT} \tag{16}$$

where ω = angular frequency; $\hbar = h/2\pi$ (where h is Planck's constant); $N = nZ$ = number of atoms in the primitive cell; and q = total proportion of vibrational modes ascribed to Einstein's oscillators.

The expression for the corresponding third-law harmonic entropy is

$$S = \frac{3R}{Z}\left(\frac{2}{\pi}\right)^3 \sum_{i=1}^{3} \int_0^{X_i} \frac{[\arcsin(X/X_i)]^2 X\, dX}{(X_i^2 - X^2)^{1/2}(e^X - 1)} - \frac{3R}{Z}\left(\frac{2}{\pi}\right)^3 \sum_{i=1}^{3} \int_0^{X_i} \frac{[\arcsin(X/X_i)]^2}{(X_i^2 - X^2)^{1/2}} \ln(1 - e^{-X})\, dX$$

TABLE 16. Parameters of the Kieffer model for the calculation of C_V and harmonic entropy for the 12 garnet end-members

Compound	Molar V (cm^3)	gfw (g)	Cell V ($cm^3 \times 10^{24}$)	Density (g/cm^3)	V_{S1} (km/s)	V_{S2} (km/s)	V_P (km/s)	V_m (km/s)	θ_D (K)	ω_1 (cm^{-1})	ω_2 (cm^{-1})	ω_3 (cm^{-1})	$\omega_{l,0}$ (cm^{-1})	$\omega_{l,K_{max}}$ (cm^{-1})	$\omega^*_{l,K_{max}}$ (cm^{-1})	ω_u (cm^{-1})	m1/m2	E1 (cm^{-1})	E2 (cm^{-1})
Pyrope	113.268	403.127	752.353	3.56	5.05	5.05	8.96	5.62	793	73	73	130	149	115.7	124.0	638	1.519	975	875
Almandine	115.272	497.753	765.667	4.32	4.68	4.68	8.42	5.21	731	68	68	122	117	103.2	78.4	635	3.491	975	875
Spessartine	118.137	495.026	784.694	4.19	4.8	4.8	8.47	5.34	743	69	69	121	113	99.6	—	631	3.434	965	865
Grossular	125.110	450.452	831.014	3.6	5.43	5.43	9.31	6.02	821	74	74	126	180	152.2	141.9	619	2.505	950	850
Uvarovite	129.953	500.481	863.179	3.85	4.89	4.89	8.6	5.44	733	71	71	124	170	143.7	—	609	2.505	930	830
Andradite	131.981	508.183	876.654	3.85	4.85	4.85	8.51	5.39	723	70	70	123	132	111.6	121.2	589	2.505	925	825
Knoringite	117.619	453.156	781.256	3.85	4.51	4.51	8.25	5.03	701	64	64	118	139	107.9	—	628	1.519	955	855
Calderite	124.588	552.757	827.546	4.44	4.22	4.22	7.67	4.7	642	59	59	108	65	57.2	—	600	3.434	940	840
Skiagite	121.554	555.484	807.395	4.57	4.1	4.1	7.62	4.58	631	58	58	108	69	60.8	—	695	3.491	950	850
Khoharite	119.444	460.858	793.376	3.86	4.47	4.47	8.16	4.98	690	64	64	116	101	78.4	—	608	1.519	950	850
Manganese chromium garnet	122.686	545.055	814.913	4.44	4.26	4.26	7.76	4.75	652	60	60	109	103	90.6	—	621	3.434	945	845
Iron chromium garnet	119.699	547.782	795.071	4.58	4.14	4.14	7.71	4.62	640	59	59	110	107	94.3	—	625	3.491	955	855

Note: $\omega^*_{l,K_{max}}$ is the lower cut-off frequency of the optic continuum optimized on the basis of the experimental value of entropy at $T = 298.15$ °C. See the text for the significance of the other terms.

$$+\frac{3R\left(1-\frac{3}{3s}-q\right)}{X_u-X_l}\int_{X_l}^{X_u}\frac{X\,dX}{(e^X-1)}$$

$$-\frac{3R\left(1-\frac{3}{3s}-q\right)}{X_u-X_l}\int_{X_l}^{X_u}\ln(1-e^{-X_E})\,dX$$

$$+\frac{3RqX_E}{(e^{X_E}-1)}-3Rq\ln(1-e^{-X_E}). \quad (17)$$

[Eq. 17 differs from the analogous expression in Kieffer (1979c) in having the difference of integration limits at denominators of third and fourth terms on the right.] The relevant input parameters of the model for the various end-members are listed in Table 16. The cut-off acoustic frequencies ω_1, ω_2, and ω_3, the mean sound velocity, V_M, and the Debye temperature, θ_D, were derived from the known acoustic properties of garnets. The velocities V_{VRH} came from Isaack and Graham (1976) for pyrope, almandine, spessartine, and grossular and from Bass (1986) for uvarovite and andradite. Because the elastic anisotropy parameter, A, of the various (isotropic) substances is close to 1,

$$A=\frac{C_{11}-C_{12}}{2C_{44}}. \quad (18)$$

It was assumed that the transverse velocities, V_{S1} and V_{S2}, and the longitudinal velocity, V_P, are equal to those of the Voigt-Reuss-Hill determinative method ($V_{VRS,S}$, $V_{VRS,P}$, respectively). The average sound velocity, V_M, was derived from the equation of Anderson (1963), which is valid for isotropic materials:

$$V_M=\left[\frac{1}{3}\left(\frac{1}{V_{S1}^3}+\frac{1}{V_{S2}^3}+\frac{1}{V_P^3}\right)\right]^{-1/3}. \quad (19)$$

The acoustic cut-off frequencies ω_1, ω_2, and ω_3 were derived from transverse and longitudinal velocities (V_i) through

$$\omega_i=V_iK_{max}=V_i\left(\frac{6\pi^2N_0}{ZV}\right)^{1/3} \quad (20)$$

where K_{max} is the maximum wave vector, the modulus of which corresponds to the radius of a sphere of the same volume as that of the Brillouin zone in reciprocal space; N_0 is Avogadro's number; Z is the number of formula units per unit cell; and V is the volume of the primitive unit cell.

Following the guidelines of Kieffer (1980), two Einstein oscillators were selected to represent the stretching modes of the tetrahedron in the band-frequency region of 800–1000 cm^{-1}. The first oscillator, E_1, has a q_1 value of 15% of the total modes, and the second one, E_2, has a q_2 of 5% of the total modes. Table 16 shows E_1 and E_2 frequencies for each end-member. Values relevant to pyrope, almandine, spessartine, grossular, and andradite are from Kieffer (1980). The Einstein oscillators for uvarovite were placed at 930 and 830 cm^{-1}, respectively (Moenke 1961; Tarte 1965; Farmer 1974).

Upper and lower cut-off frequencies in the optic continuum (ω_u and ω_l, respectively) are needed in Function 14. The adopted upper cut-off limits for almandine, spessartine, grossular, and andradite are from Kieffer (1980). The value of ω_u for pyrope was adjusted from that used by Kieffer (1980) to 638 cm^{-1} (Bokreta 1992), and the value for uvarovite was set at 609 cm^{-1} (Moenke 1961; Tarte 1965; Farmer 1974). The ω_l limit is the most critical parameter for the estimation of macroscopic thermodynamic functions. Values of ω_l at $K = 0$ (center of the Brillouin zone) on the basis of infrared spectra are related to those at $K = K_{max}$ through

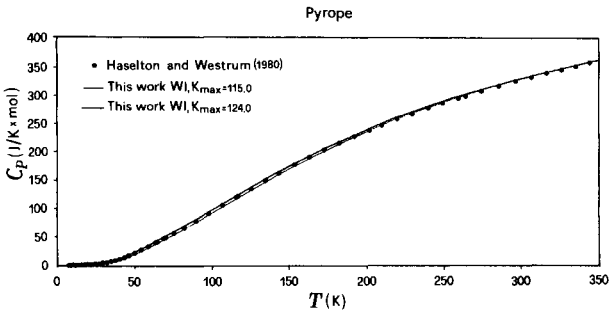

FIGURE 8. Comparison of isobaric heat capacity of pyrope, calculated according to Kieffer's model, with low-T calorimetric data.

$$\omega_{1,K_{max}} = \omega_{1,K=0}\left(1 + \frac{m_2}{m_1}\right)^{-1/2} \quad (21)$$

where m_1 and m_2 are the reduced masses of the ions (O and "heavy" cation, respectively, in our case; see Kieffer 1980). The $\omega_{1,K_{max}}$ values for pyrope, almandine, spessartine, grossular, and andradite are from Kieffer (1980). For uvarovite a value of 170 cm^{-1} for $\omega_{1,K=0}$ was estimated from the spectrum of Moore et al. (1971), and the corresponding $\omega_{1,K_{max}}$ was obtained by application of Equation 21.

The model parameters for the uncommon garnet endmembers were obtained by Bokreta (1992) through linear regression involving the atomistic properties of the elements and are here so retained. Expressions 13–15 and the various terms in Equation 17 were then calculated by Gaussian integration. Values of the nondimensionalized frequencies $\omega_{1,K_{max}}$ were adjusted from the initial input values by a trial-and-error procedure to obtain a match between the calculated values of S_V and experimental third-law entropy values at T = 298.15 K, P = 1 bar. Corrections were made for a magnetic-spin entropy contribution of the form

$$S_m = \mathrm{R}\ln(2q + 1) \quad (22)$$

where q is 3/2 for Cr^{3+}, 5/2 for Mn^{2+} and Fe^{3+}, 2 for Fe^{2+}, and for anharmonicity, according to

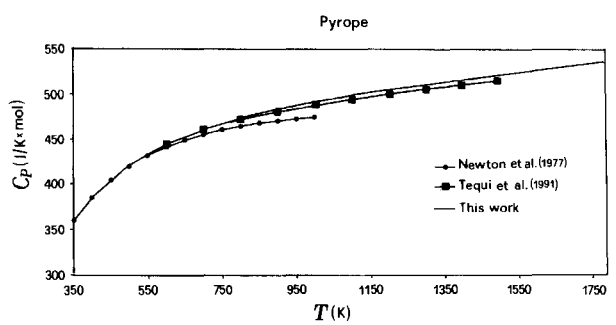

FIGURE 9. Comparison of heat capacity of pyrope at constant P, calculated according to Kieffer's model, with high-T calorimetric data.

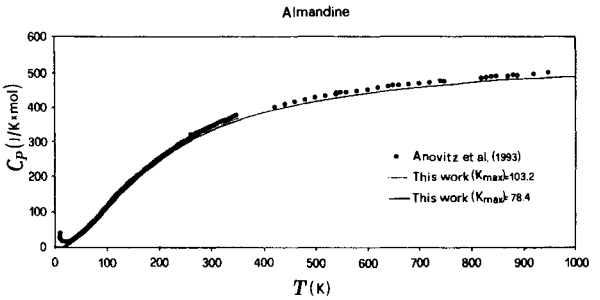

FIGURE 10. C_P predictions for almandine on the basis of Kieffer's model in comparison with experimental data.

$$S_{an} = \int_0^T V\alpha^2 K_0 \, dT. \quad (23)$$

Our procedure is operationally different from the one indicated by Kieffer (1980), who fitted calculated C_V at 100 K to the calorimetric C_P after subtraction of the contribution from thermal expansion:

$$C_P = C_V + TV\alpha^2 K_0. \quad (24)$$

Figure 8 shows how calculated C_P values for pyrope compare with the low-T calorimetric measurements of Haselton and Westrum (1980). Adopting the initial guess value of $\omega_{1,K_{max}}$ (115.7 cm^{-1}; see Table 16) leads to an entropy estimate at T_r = 298.15 of 272.15 J/(mol·K) (268.834 harmonic + 3.316 anharmonic). Because the calorimetric value is 266.27, the initial guess value of $\omega_{1,K_{max}}$ is too low and must be increased to 124.0 cm^{-1} to match the calorimetric datum. As we see in Figure 8, the resulting C_P in the low-T region also compares better with calorimetric values after adjustment of the nondimensionalized frequency at the limit of the Brillouin zone. In Figure 9, model predictions for pyrope are compared with high-T calorimetric data of Newton et al. (1977) and Tequi et al. (1991), indicating a reasonable agreement with this last source. The model calculations for almandine with the initial guess value of $\omega_{1,K_{max}}$ = 103.2 cm^{-1} lead to $S_{298.15}$ = 322.051 J/(mol·K) (279.625 harmonic + 2.28 anharmonic + 40.146 magnetic), which is rather low in comparison with the calorimetric value (342.6; Anovitz et al. 1993). To fit the calorimetric third-law entropy, $\omega_{1,K_{max}}$ must

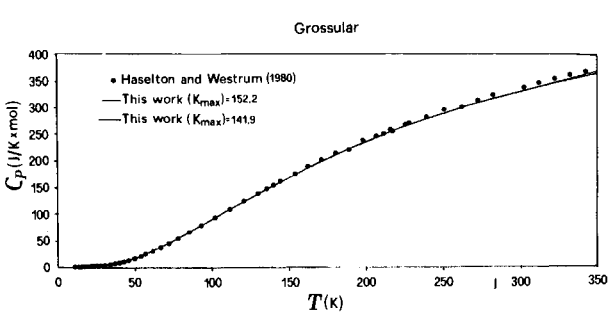

FIGURE 11. C_P predictions for grossular on the basis of Kieffer's model in comparison with experimental data.

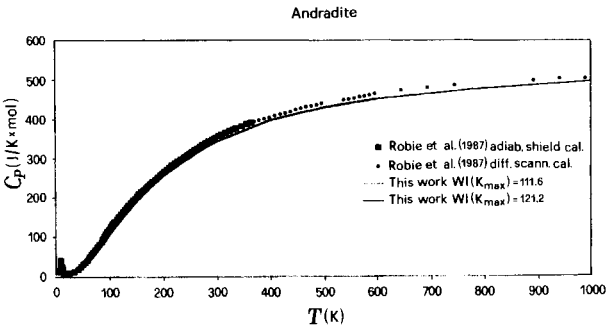

FIGURE 12. C_P predictions for andradite on the basis of Kieffer's model in comparison with experimental data.

be lowered to 78.4 cm^{-1}. As shown in Figure 10, the calculated heat-capacity function obviously does not reproduce the effects of the antiferromagnetic-paramagnetic lambda transition experimentally observed at 8.7 K; the high-T estimates are, however, not far from the calorimetric measurements after magnetic spin + anharmonicity corrections. The model estimates for grossular agree very well with the low-T experimental data of Haselton and Westrum (1980) (Fig. 11). To match the calorimetric entropy [$S_{298.15}$ = 260.12 J/(mol·K); Haselton and Westrum 1980], $\omega_{1,K_{max}}$ must be lowered to 141.9 cm^{-1} from the initial guess value of 152.2 cm^{-1} (Table 16). The initial estimate for andradite gave $S_{298.15}$ = 323.714 J/(mol·K) (290.744 harmonic + 3.174 anharmonic + 29.796 magnetic) in comparison with the experimental third-law value of 316.4 J/(mol·K) (Robie et al. 1987). To match this value, $\omega_{1,K_{max}}$ must be increased to 121.2 from the initial 111.6 cm^{-1}. The resulting C_P curve (Fig. 12) at high T remains, however, slightly lower with respect to adiabatic shielding and differential scanning calorimetric values. Because there are no sufficiently accurate calorimetric values with which to compare the remaining compositional terms, we retained the initial guess value of $\omega_{1,K_{max}}$ resulting from Relationship 21. We present in Table 17 the complete results for all 12 end-members of interest in this study. As a result of the fitting procedure the accuracy of the proposed standard-state entropy value would be approximately 7 J/(mol·K) for Fe-free components.

SUMMARY AND CONCLUSIONS

This contribution was not intended to fulfill the ambitious goal of solving garnet energetics but simply to focus attention on the deep interconnection existing among thermophysical parameters, which cannot be treated, as is often done, as mutually independent fitting variables.

One can parameterize the cohesive energy (U) for a cubic solid in the framework of the Born model by comparing the experimentally observed pressure-volume relationship (P-V) in a wide range of P conditions with the corresponding U and V variations at constant temperature (T). Under hydrostatic pressure

$$P = -\left(\frac{\partial F}{\partial V}\right) \tag{25}$$

where F is the Helmholtz free energy:

$$F(V, T) = U(V) + F_{vib}(V, T). \tag{26}$$

In the harmonic approximation the vibrational part of the Helmholtz free energy of the solid (F_{vib}) does not de-

TABLE 17. Third-law entropy and heat-capacity function for the various garnet end-members in comparison with calorimetric values

Name	Formula	S_v	S_{anh}	S_{mag}	S	$C_P = A + BT + CT^{-2} + DT^{-1/2} + ET^2$					T range	Ref.
						$A \times 10^{-2}$	$B \times 10$	$C \times 10^{-5}$	$D \times 10^{-3}$	$E \times 10^{5}$		
Pyrope	$Mg_3Al_2Si_3O_{12}$	262.967	3.316	0	266.283	8.7293	−1.4750	−4.7243	−8.6643	4.1084	298.15–m.p.	1
					266.27	8.025	−0.958	−23.52	−7.2877	0	350–1000	2, 3
						8.72988	−1.3744	0.045	−8.7943	3.3408	820–1300	4
Almandine	$Fe_3Al_2Si_3O_{12}$	300.136	2.280	40.146	342.562	8.7094	−1.6067	−1.6953	−8.5176	5.2364	298.15–m.p.	1
					342.6	2.9274	3.4652	−72.099	0.7163	15.317	400–1000	5
Spessartine	$Mn_3Al_2Si_3O_{12}$	283.960	2.845	44.694	331.499	8.7486	−1.4680	−4.7045	−8.6060	4.0201	298.15–m.p.	1
Grossular	$Ca_3Al_2Si_3O_{12}$	257.830	2.295	0	260.125	8.7296	−1.4846	−4.6095	−8.6330	3.9643	298.15–m.p.	1
					260.12							2
Uvarovite	$Ca_3Cr_2Si_3O_{12}$	260.659	3.098	23.053	286.81	8.7266	−1.4730	−3.1499	−8.5940	4.0649	298.15–m.p.	1
Andradite	$Ca_3Fe_2Si_3O_{12}$	283.455	3.174	29.796	316.425	8.7479	−1.4858	3.4215	−8.6066	4.1040	298.15–m.p.	1
					316.4	8.0924	−0.7025	−6.789	−7.403	0	300–1000	6
Knoringite	$Mg_3Cr_2Si_3O_{12}$	279.186	2.931	23.053	305.17	8.7557	−1.4656	−4.5706	−8.6212	4.0758	298.15–m.p.	1
Calderite	$Mn_3Fe_2Si_3O_{12}$	336.223	3.875	74.490	414.588	8.7683	−1.4606	6.9140	−8.5977	4.1656	298.15–m.p.	1
Skiagite	$Fe_3Fe_2Si_3O_{12}$	296.613	3.316	69.942	369.871	8.7074	−1.4476	−4.0045	−8.6526	4.3207	298.15–m.p.	1
Khoharite	$Mg_3Fe_2Si_3O_{12}$	311.215	3.406	29.796	344.417	8.7616	−1.4715	5.2712	−8.6516	4.2446	298.15–m.p.	1
Manganese chromium garnet	$Mn_3Cr_2Si_3O_{12}$	296.140	3.904	67.747	367.791	8.7736	−1.4637	5.2303	−8.6415	4.2123	298.15–m.p.	1
Iron chromium garnet	$Fe_3Cr_2Si_3O_{12}$	291.425	3.331	63.199	357.955	8.7447	−1.4813	−1.5757	−8.5953	4.0796	298.15–m.p.	1

Note: References are as follows: 1 = this work, 2 = Haselton and Westrum (1980), 3 = Newton et al. (1977), 4 = Tequi et al. (1991), 5 = Anovitz et al. (1993), 6 = Robie et al. (1987). Temperature is in kelvins. Entropy and the heat-capacity function are in joules per mole-kelvin.

TABLE 18. Thermodynamic properties of end-member garnets according to the present study

Compound	H (kJ/mol)	S [J/(mol·K)]	G (kJ/mol)	V (cm³)	C_p [J/(mol·K)] $A \times 10^{-2}$	$B \times 10$
Pyrope	−6290.760	266.283	−6370.152	113.268	8.7293	−1.4750
Almandine	−6261.300	342.562	−5363.435	115.272	8.7094	−1.6067
Spessartine	−5686.934	331.499	−5785.770	118.137	8.7486	−1.4680
Grossular	−6632.760	260.125	−6710.316	125.110	8.7296	−1.4846
Uvarovite	−6034.580	286.810	−6120.092	129.953	8.7266	−1.4730
Andradite	−5758.850	316.425	−5853.193	131.981	8.7479	−1.4858
Knoringite	−5576.077	305.170	−5667.064	117.619	8.7557	−1.4656
Calderite	−4719.777	414.588	−4843.386	124.588	8.7683	−1.4606
Skiagite	−4276.224	369.871	−4386.501	121.554	8.7074	−1.4476
Khoharite	−5299.472	344.417	−5402.160	119.444	8.7616	−1.4715
Manganese chromium garnet	−5007.081	367.791	−5116.737	122.686	8.7736	−1.4637
Iron chromium garnet	−4555.256	357.955	−4661.980	119.699	8.7447	−1.4813

pend explicitly on the volume. This fact and the further assumption that F_{vib} is a purely T-dependent function lead to the Hildebrand equation of state (EOS):

$$\frac{\partial U}{\partial V} = -P + T\alpha K_0 \tag{27}$$

$$V\frac{\partial^2 U}{\partial V^2} = K_0 + TK_0^2(K_T^1 + K_0K_P^1). \tag{28}$$

Neglecting the vibrational contribution to the thermodynamic functions of the solid (i.e., treating the solid as purely static, cf. Tosi 1964) or operating at constant T reduces Equations 27 and 28 to the simple form

$$\frac{\partial U}{\partial V} = -P \tag{29}$$

$$V\frac{\partial^2 U}{\partial V^2} = K_0. \tag{30}$$

The development of a structural model for garnets based on Novak-Gibbs–type expressions, appropriate crystal radii, and DLS refinement allows the evaluation of the compressional behavior and the thermal expansion of the various end-members in the system $(Ca,Mg,Mn,Fe)_3(Al,Cr,Fe)_2SiO_3O_{12}$. After definition of EOS parameters, the compressional work was equated to the increase of internal energy when operating at constant T. It was thus shown that all end-members in the above system have short-range repulsive energies consistent with a hardness factor ρ in the range 0.45–0.51 Å. For a given component it was shown that the ρ factor cannot be assumed to be constant for a wide P range. Adopting (within the approximations of the method) a common ρ factor (0.48 Å) for all compounds in the family of salts (Huggins-Mayer approach) and assuming, as a first approximation, the repulsive radii to be coincident with the crystal radii, it was shown that the common garnet end-members are close to the Born-Mayer condition (constant preexponential b factor for all salts in a family of isostructural compounds). The static energies of the common end-members were then reproduced, on the basis of calorimetric enthalpy at standard state, through Born-Haber-Fayans thermochemical calculations, and by solving for the repulsive terms under the ideal condition of constant b and constant ρ for all compounds (the combined Huggins-Mayer Born-Mayer approach). Inasmuch as all end-members are rigorously coplanar in the chemical space of interest, and because all elements are present in the common compounds, the derivation of appropriate repulsive radii consistent with the above approach allowed the derivation of standard-state enthalpy values for the uncommon compositional terms.

Application of the Kieffer model of vibrational energy, with an appropriate parameterization of the lower cut-off frequency of the optical continuum, allowed an estimate of the harmonic heat-capacity function and the harmonic entropy. The knowledge of the isobaric thermal expansion and isothermal compressibility coefficients previously calculated for the various compounds allowed an estimate of anharmonic contributions to the vibrational energy. The heat capacity at constant P and the standard-state third-law entropy of the various salts were thus derived. The obtained thermodynamic parameters for the 12 garnet end-members are summarized in Table 18. The listed values are mutually and internally consistent and reproduce well the experimental mean values hitherto proposed for this class of solids.

ACKNOWLEDGMENTS

This work benefited considerably from discussions with scientists attending the "Workshop on the Crystal-Chemistry of Garnets" held in Villasimius (Italy) under the sponsorship of MURST Strategic Project "Cristallochimica e Termodinamica dei Minerali." Thanks are due to Charles Geiger for comments and suggestions on a preliminar draft of the manuscript and to Jibamitra Ganguly and an anonymous reviewer for careful formal reviews.

REFERENCES CITED

Abraham, S.C., and Geller, S. (1958) Refinement of the structure of a grossularite garnet. Acta Crystallographica, 11, 437–441.

Anderson, O.L. (1963) A simplified method for calculating the Debye temperature from elastic constants. Journal of Physical Chemistry of Solids, 24, 909–917.

Anovitz, L.M., Essene, E.J., Metz, G.W., Bohlen, S.R., Westrum, E.F., Jr., and Hemingway, B.S. (1993) Heat capacity and phase equilibria of

TABLE 18.—*Continued*

C_p [J/(mol·K)]			α[K^{-1}]			K[Mbar]	
$C \times 10^{-5}$	$D \times 10^{-3}$	$E \times 10^{5}$	$\alpha_0 \times 10^{5}$	$\alpha_1 \times 10^{9}$	α_2	K_0	K'
−4.7243	−8.6643	4.1084	2.431	5.649	−0.2205	1.77604	4.78450
−1.6953	−8.5176	5.2364	1.781	11.558	−0.2000	1.83755	4.79524
−4.7045	−8.6060	4.0201	2.962	2.398	−0.8122	1.79731	4.83388
−4.6095	−8.6330	3.9643	2.224	5.272	−0.4119	1.67384	4.88739
−3.1499	−8.5940	4.0649	2.232	5.761	−0.2329	1.74317	4.97774
3.4215	−8.6066	4.1040	2.208	6.019	−0.2005	1.72659	4.90955
−4.5706	−8.6212	4.0758	2.894	2.9642	−0.7748	1.87573	4.84250
−6.9140	−8.5977	4.1656	2.898	3.7316	−0.5455	1.81769	4.82315
−4.0045	−8.6526	4.3207	2.336	7.0286	−0.2950	1.6692	4.76181
5.2712	−8.6516	4.2446	2.626	5.3687	−0.4521	1.85660	4.79862
5.2303	−8.6415	4.2123	2.862	4.0015	−0.5160	1.85174	4.89417
−1.5757	−8.5953	4.0796	2.584	3.7865	−0.4282	1.90211	4.83062

almandine, $Fe_3Al_2Si_3O_{12}$. Geochimica et Cosmochimica Acta, 57, 4191–4204.

Armbruster, T., Geiger, C.A., and Lager, G.A. (1992) Single-crystal X-ray structure study of synthetic pyrope almandine garnets at 100 and 293 K. American Mineralogist, 77, 512–521.

Armbruster, T., and Geiger, C. (1993) Andradite crystal chemistry, dynamic-site disorder and structural strain in silicate garnets. European Journal of Mineralogy, 5, 59–71.

Babuska, V., Fiala, J., Rumazawa, M., Ohno, I., and Sumino, Y. (1978) Elastic properties of garnet solid-solution series. Physics of the Earth and Planetary Interiors, 16, 157–176.

Baerlocher, C., Hepp, A., and Meier, W.M. (1977) DLS-76: A program for the simulation of crystal structures by geometric refinement. Institute of Crystallography and Petrography, Eidgenössiche Technische Hochschule, Zurich, Switzerland.

Barin, I., Knacke, O., and Kubaschewsky, O. (1977) Thermochemical properties of inorganic substances: Supplement, 861 p. Springer, Berlin.

Bass, J.D. (1986) Elasticity of uvarovite and andradite garnets. Journal of Geophysical Research, 91, 7505–7516.

——— (1989) Elasticity of grossular and spessartite garnets by Brillioun spectroscopy. Journal of Geophysical Research, 94, 7621–7628.

Bassett, W.A., and Takahashi, T. (1974) X-ray diffraction studies up to 300 kbar. In R.H.L. Wendorf, Ed., Advances in high-pressure research, vol. 4, p. 165–247. Academic, New York.

Basso, R. (1985) Crystal chemical and crystallographic properties of compounds with garnet or hydrogarnet structure. Neues Jahrbuch für Mineralogie Monatshefte, 3, 108–114.

Baur, W.H. (1971) The prediction of bond length variations in silicon-oxygen bonds. American Mineralogist, 56, 1573–1599.

——— (1972) Computer-simulated crystal structures of observed and hypothetical Mg_2SiO_4 polymorphs of low and high density. American Mineralogist, 57, 709–731.

——— (1977) Computer-simulated crystal structures. Physics and Chemistry of Minerals, 2, 3–20.

——— (1981) Interatomic distance predictions for computer simulation of crystal structures. In M. O'Keeffe and A. Navrotsky, Eds., Structure and bonding in crystals, vol. II, p. 31–52. Academic, New York.

Berman, R.G. (1988) Internally consistent thermodynamic data for minerals in the system Na_2O-K_2O-CaO-MgO-FeO-Fe_2O_3-Al_2O_3-SiO_2-TiO_2-H_2O-CO_2. Journal of Petrology, 29, 445–522.

——— (1990) Mixing properties of Ca-Mg-Fe-Mn garnets. American Mineralogist. 75, 328–344.

Bertaut, F., and Forrat, F. (1957) Garnet parameters. Comptes Rendue de l'Academie de France, 244, 96–99.

Bhattacharya, A. (1986) Some geobarometers involving cordierite in the FeO-Al_2O_3-SiO_2 ($\pm H_2O$) system: Refinements, thermodynamics, calibration, and application in granulite facies rocks. Contributions to Mineralogy and Petrology, 94, 387–394.

Boeglin, M. (1981) Mineralogie et géochimie des gisements de manganèse de Conselheiro Lafaieteau Brésil et de Moanda au Gabon. Thèse de 3me cycle, Toulouse, France.

Bokreta, M. (1992) Energetics of garnets: Computational model of the thermochemical and thermophysical properties. Ph.D. dissertation. University of Pennsylvania, Philadelphia.

Bonczar, L.T., Graham, E.K., and Wang, H. (1977) The pressure and temperature dependence of the elastic constants of pyrope garnets. Journal of Geophysical Research, 82, 2529–2534.

Catti, M. (1978) Electrostatic lattice energy in ionic crystals: Optimization of the convergence of Ewald series. Acta Crystallographica, A34, 974–979.

——— (1981) A generalized Born-Mayer parameterization of the lattice energy in orthorhombic ionic crystals. Acta Crystallographica, A37, 72–76.

Charlu, T.V., Newton, R.C., and Kleppa, O.J. (1975) Thermochemistry of high-pressure garnets and clinopyroxenes in the system CaO-MgO-Al_2O_3-SiO_2 from high-temperature solution calorimetry. Geochimica et Cosmochimica Acta, 39, 1487–1497.

Charlu, T.V., Newton, R.C., and Kleppa, O.J. (1978) Enthalpy of formation of lime silicates by high temperature calorimetry, with discussion of high pressure phase equilibrium. Geochimica et Cosmochimica Acta, 42, 367–375.

Chatillon-Colinet, C., Kleppa, O.J., Newton, R.C., and Perkins, D., III (1983) Enthalpy of formation of $Fe_3Al_2Si_3O_{12}$ (almandine) by high temperature alkali borate solution calorimetry. Geochimica et Cosmochimica Acta, 47, 439–444.

Chatterjee, N. (1987) Evaluation of thermochemical data on Fe-Mg olivine, orthopyroxene, spinel and Ca-Fe-Mg-Al garnet. Geochimica et Cosmochimica Acta 51, 2515–2525.

Della Giusta, A., and Ottonello, G. (1993) Energy and long-range disorder in simple spinels. Physics and Chemistry of Minerals, 20, 228–241.

Duba, A., and Olinger, S. (1972) Compression of garnet to 100 kilobars. Journal of Geophysical Research, 77, 2496–2499.

Farmer, V.C. (1974) The infrared spectra of minerals. Mineralogical Society Monograph 4, 539 p. Mineralogical Society, London, U.K.

Fed'kin, V.V. (1970) Calculation of mineral equilibria in the iron (II) oxide-alumina-silica-oxygen system. Geologicheskij Geofiziki, 12, 22–38.

Fursenko, S.A. (1981) High pressure synthesis of the new chromium bearing garnet $Mg_3Cr_2Si_3O_{12}$. Doklady, Academy of Sciences, USSR, 250, 176–179.

Ganguly, J., Cheng, W., and O'Neill, H.St.C. (1993) Syntheses, volume, and structural changes of garnets in the pyrope-grossular join: Implications for stability and mixing properties. American Mineralogist, 78, 583–593.

Geiger, C.A., Krause, C., Ross, C.R., Jr., Amthauer, G., and Langer, K. (1989a) Characterization of almandine, pyrope, pyrope-almandine and pyrope-grossular solid solutions. Terra Abstract, 1, 290.

Geiger, C.A., Winkler, B., and Langer, K. (1989b) Infrared spectra of synthetic almandine-grossular and almandine-pyrope solid solutions: Evidence for equivalent site behavior. Mineralogical Magazine, 53, 231–237.

Gibbs, G.V., and Smith, J.V. (1965) Refinement of the crystal structure of synthetic pyrope. American Mineralogist, 50, 2023–2039.

Gnevushev, M.A., Kalinin, A.I., Mikheev, V.I., and Smirnov, G.I. (1956) Change in the cell dimensions of the garnets as a function of their chemical composition. Zapiski Vsesoyuznogo Mineralogicheskogo Obshchestva, 85, 472–490.

Greenwood, N.N. (1970) Ionic crystals, lattice defects and nonstoichiometry, 194 p. Chemical Publishing Company, New York.

Grover, R., Getting, C., and Kennedy, G.C. (1973) Simple compressibility relations for solids. Physical Review B, 7, 567–571.

Guigas, B. (1975) Verfeinerung von Kristallstructuren mit dem Distance Least Squares-Verfahren: Sehndlung von Konvergenzfragen und kristtallographische Anwendungen. Doctoral dissertation, University of Karlsruhe, Germany.

Gustafson, W.I. (1974) The stability of andradite, hedenbergite and related minerals in the system Ca-Fe-Si-O-H. Journal of Petrology, 15, 455–496.

Halleck, P.M. (1973) The compression and compressibility of grossularite garnet: A comparison of X-ray and ultrasonic methods. Ph.D. thesis, University of Chicago, Illinois.

Harlow, D.E., and Newton, R.C. (1992) Experimental determination of the reaction 2 magnetite + 2 kyanite + 4 quartz in the FeO-CaO-Al_2O_3-SiO_2-H_2O system. Geochemistry International, 23(6), 158–169.

Haselton, H.T., and Westrum, E.F. (1980) Low-temperature heat capacities of synthetic pyrope, grossular, and $pyrope_{60}grossular_{40}$. Geochimica et Cosmochimica Acta, 44, 701–709.

Hawthorne, F.C. (1981) Some systematics of the garnet structure. Journal of Solid State Chemistry, 37, 157–164.

Hazen, R.M., and Prewitt, C.T. (1977) Effects of temperature and pressure on interatomic distances in oxygen-based minerals. American Mineralogist, 62, 309–315.

Hazen, R.M., and Finger, L.W. (1978) Crystal structures and compressibilities of pyrope and grossular to 60 kbar. American Mineralogist, 63, 297–303.

——— (1979) Bulk modulus-volume relationship for cation-anion polyhedra. Journal of Geophysical Research, 84, 6723–6728.

——— (1982) Comparative crystal chemistry, 229 p. Wiley, New York.

——— (1989) High-pressure crystal chemistry of andradite and pyrope: Revised procedures for high-pressure diffraction experiments. American Mineralogist, 74, 352–359.

Helgeson, H.C., Delany, J.M., Nesbitt, H.W., and Bird, D.K. (1978) Summary and critique of thermodynamic properties of rock-forming minerals. American Journal of Science, 278A, 1–229.

Holland, T.J.B., and Powell, R. (1990) An enlarged and updated internally consistent thermodynamic dataset with uncertains and correlations: The system K_2-Na_2O-CaO-MgO-MnO-FeO-Fe_2O_3-Al_2O_3-TiO_2-SiO_2-C-H_2-O_2. Journal of Metamorphic Geology 8, 89–124.

Hsu, L.C. (1968) Selected phase relationships in the system Al-Mn-Fe-Si-O-H: A model for garnet equilibria. Journal of Petrology, 9, 40–83.

Hukenholtz, H.G., and Knittel, D. (1975) Uvarovite: Stability of uvarovite-grossularite solid solutions at low pressure. Contributions to Mineralogy and Petrology, 49, 211–232.

Irifune, T., Ohtani, E., and Kumazawa, M. (1982) Stability field of knorringite $Mg_3Cr_2Si_3O_{12}$ at high pressure and its application to the occurrence of chromium-rich pyrope in the upper mantle. Physics of the Earth and Planetary Interiors, 27, 263–272.

Isaack, D.G., and Graham, E.K. (1976) The elastic properties of an almandine-spessartine garnet and elasticity in the garnet solid solution series. Journal of Geophysical Research, 81, 2483–2489.

Isaak, G., Anderson, L., and Oda, H. (1992) High-temperature thermal expansion and elasticity of calcium-rich garnets. Physics and Chemistry of Minerals, 19, 106–120.

Karpinskaya, T.B., Ostrovskiy, I.A., and Yevstigneyeva, T.L. (1983) Synthetic pure iron garnet skiagite. International Geological Review, 25, 1129–1130.

Karpov, I.K., and Kashik, S.A. (1968) Computer calculation of standard isobaric-isothermal potentials of silicates by multiple regression from a crystallochemical classification. Geokhimiya, 7, 806–814.

Karpov, I.K., Kiselev, A.I., and Letnikov, F.A. (1971) Chemical thermodynamics in petrology and geochemistry, 385 p. Nauka, Irkutsk, Russia.

——— (1976) Modellization of natural mineral structures, 254 p. Niedra, Moscow.

Karpov, I.K., Dorogekopets, P.I., and Lashkevich, V.V. (1977) Optimal errors thermodynamic characteristics of rock forming minerals according to minimax criterion. In L.V. Tauson, Ed., Geochemistry of endogenic processes, p. 196–202. Nauka, Irkutsk, Russia.

Kawasaki, T., and Matsui, Y. (1977) Partitioning of Fe^{2+} and Mg between olivine and garnet. Earth and Planetary Science Letters, 37, 159–166.

Kieffer, S.W. (1979a) Thermodynamics and lattice vibrations of minerals: 1. Mineral heat capacities and their relationships to simple lattice vibrational model. Review of Geophysics and Space Physics, 17, 1–19.

——— (1979b) Thermodynamics and lattice vibrations of minerals: 2. Vibrational characteristics of silicates. Review of Geophysics and Space Physics, 17, 20–34.

——— (1979c) Thermodynamics and lattice vibrations of minerals: 3. Lattice dynamics and an approximation for minerals with application to simple substances and framework silicates. Review of Geophysics and Space Physics, 17, 35–59.

——— (1980) Thermodynamics and lattice vibrations of minerals: 4. Application to chain and sheet silicates and orthosilicates. Review of Geophysics and Space Physics, 18, 862–886.

——— (1982) Thermodynamics and lattice vibrations of minerals: 5. Application to phase equilibria, isotopic fractionation and high-pressure thermodynamic properties. Review of Geophysics and Space Physics, 20, 827–849.

Kiseleva, I.A. (1976) Thermodynamic properties and stability of pyrope. Geokhimiya, 6, 845–854.

——— (1977) Gibbs free energy of formation of calcium garnets. Geokhimiya, 5, 705–715.

Kiseleva, I.A., Topor, N.D., and Mel'chakova, L.V. (1972) Experimental determination of heat content and heat capacity of grossularite, andradite and pyrope. Geokhimiya, 11, 1372–1379.

Kohn, M.J., and Spear, F.S. (1991) Error propagation for barometers: 1. Accuracy and precision of experimentally located end-member reactions. American Mineralogist, 76, 128–137.

Lattard, D., and Schreyer, W. (1983) Synthesis and stability of the garnet calderite in the system Fe-Mn-Si-O. Contributions to Mineralogy and Petrology, 84, 199–214.

Leger, J.M., Redon, A.M., and Chateau, C. (1990) Compression of synthetic pyrope, spessartite and uvarovite up to 25 GPa. Physics and Chemistry of Minerals, 17, 161–167.

Leitner, J.B., Weidner, D.J., and Liebermann, R.C. (1980) Elasticity of single crystal pyrope and implications for garnet solid-solution series. Physics of the Earth and Planetary Interiors, 22, 111–121.

Levien, L., Prewitt, C.T., and Weidner, D.J. (1978) Comparison of determinations of bulk moduli for pyrope. Eos, 59, 1180.

Liou, J.G. (1974) Stability relations of andradite-quartz in the system Ca-Fe-Si-O-H. American Mineralogist, 59, 1016–1025.

McConnell, D. (1966) Proprietes physiques des grenats: Calcule de la dimension de la maille unite a partir de chimique. Geochimica et Cosmochimica Acta, 31, 1479–1487.

Meagher, E.P. (1975) The crystal structures of pyrope and grossularite at elevated temperatures. American Mineralogist, 60, 218–228.

Meier, W.M., and Villiger, H. (1969) Die methode der abstandsverfeinerung zur bestimmung der atomkoordinaten idealisierter geruststruckturen. Zeitschift für Kristallographie, 129, 411–423.

Menzer, G. (1926) Die kristallstructure von granat. Zeitschift für Kristallographie, 63, 157–158.

Moenke, H. (1961) Differentiation of garnet minerals in the infrared region 400–650 cm^{-1}. VEB Carl Zeiss Jena Nachrickten, 9, 82–90.

Moore, R.K., White, W.B., and Long, T.V. (1971) Vibrational spectra of the common silicates: I. The garnets. American Mineralogist, 56, 54–71.

Newton, R.C., Charlu, T.V., and Kleppa, O.J. (1977) Thermochemistry of high pressure garnets and clinopyroxenes in the system CaO-MgO-Al_2O_3-SiO_2. Geochimica et Cosmochimica Acta, 41, 369–377.

Novak, G.A., and Gibbs, G.V. (1971) The crystal chemistry of silicate garnets. American Mineralogist, 56, 791–825.

O'Neill, B., Bass, J.D., Rossman, G.R., Geiger, C.A., and Langer, K. (1991) Elastic properties of pyrope. Physics and Chemistry of Minerals, 17, 617–621.

Ostrovskii, I.A. (1990) Isobaric potential of some garnets at temperature up to 4000K and pressure 1000 kbar. Izvestia Akademia Nauka SSSR, Series Geology, 8, 13–20.

Ottonello, G. (1987) Energies and interactions in binary (*Pbnm*) orthosilicates: A Born parameterization. Geochimica et Cosmochimica Acta, 51, 3119–3135.

——— (1992) Interactions and mixing properties in the (*C2/c*) clinopyroxene quadrilateral. Contributions to Mineralogy and Petrology, 111, 53–60.

Ottonello, G., Pricivalle, F., and Della Giusta, A. (1990) Temperature, composition and f_{O_2} effects on intersite distribution of Mg and Fe^{2+} in olivines. Physics and Chemistry of Minerals, 17, 301–312.

Ottonello, G., Della Giusta, A., Dal Negro, A., and Baccarin, F. (1992) A structure-energy model for *C2/c* pyroxenes in the system Na-Mg-Ca-Mn-Fe-Al-Cr-Ti-Si-O. In Advances in Physical Geochemistry, 10, 194–238.

Pauling, L. (1960) The nature of the chemical bond, 644 p. Cornell University Press, Ithaca, New York.

Prandl, W. (1966) Verfeinerung der Grossulars mit Neutronen und Roentgenstrahlbeugung. Zeitschift für Kristallographie, 123, 81–116.

——— (1971) Die magnetische struktur und die atom parameter des almandines $Al_2Fe_3(SiO_4)_3$. Zeitschift für Kristallographie, 134, 333–334.

Quareni, S., and De Pieri, R. (1966) La stucttura dell'andradite. Memorie dell'Accademia Patavina di Scienze Lettere ed Arti, 78, 153–164.

Rakai, R.J. (1975) Crystal structure of spessartine and andradite at elevated temperatures. M.Sc. thesis, University of British Columbia, Vancouver.

Rickwood, P.C. (1969) On recasting analyses of garnet into end-member molecules. Contributions to Mineralogy and Petrology, 18, 175–198.

Robie, R.A., Bethke, P.M., and Beardsley, K.M. (1967) Selected X-ray crystallographic data, molar volumes, and densities of minerals and related substances. U.S. Geological Survey Bulletin, 1248.

Robie, R.A., Hemingway, B.S., and Fisher, J.R. (1978) Thermodynamic properties of minerals and related substances at 298.15 K and 1 bar (105 pascals) pressure and at higher temperatures. U.S. Geological Survey Bulletin, 1452.

Robie, R.A., Bin, Z., Hemingway, B.S., and Barton, M.D. (1987) Heat capacity and thermodynamic properties of andradite garnets, $Ca_3Fe_2Si_3O_{12}$, between 10 and 1000 K and revised values for $\Delta_f G^\circ_m$ (298.15 K) of hedembergite and wollastonite. Geochimica et Cosmochimica Acta, 51, 2219–2236.

Sato, Y., Akaogi, M., and Akimoto, S. (1978) Hydrostatic compression of the synthetic garnets pyrope and almandine. Journal of Geophysical Research, 83B, 335–338.

Shannon, R.D. (1976) Revised effective ionic radii and systematic studies of interatomic distances in halides and calcogenides. Acta Crystallographica, A32, 751–767.

Shannon, R.D., and Prewitt, C.T. (1969) Effective ionic radii in oxides and fluorides. Acta Crystallographica, B25, 925–946.

Skinner, B.J. (1956) Physical properties of end-members of the garnet group. American Mineralogist, 41, 428–436.

Sobolev, N.V. (1974) Deep-seated inclusions in kimberlites and the problem of composition of the upper mantle. Nauka, Novosibirsk, Russia.

Sumino, Y., and Nishizawa, O. (1978) Temperature variation of elastic constants of pyrope-almandine garnets. Journal of Physical Earth, 26, 239–252.

Suwa, Y., Tami, Y., and Naka, S. (1976) Stability of synthetic andradite at atmospheric pressure. American Mineralogist, 61, 26–28.

Suzuki, I., and Anderson, O.L. (1983) Elasticity and thermal expansion of a natural garnet up to 1000 K. Journal of Physical Earth, 31, 125–138.

Takahashi, T., and Liu, L. (1970) Compression of ferromagnesian garnets and the effect of solid-solutions on the bulk modulus. Journal of Geophysical Research, 75, 5757–5766.

Tarte, P. (1965) Experimental study and interpretation of infrared spectra of silicates and germanates. Memorires de Academie Royal Belgique Cl. Sciences 8° 35, parts 4a, 4b.

Tarte, P., and Deliens, M. (1973) Correlation between infrared spectrum and the composition of garnets in the pyrope-almandine-spessartite series. Contributions to Mineralogy and Petrology, 40, 25–37.

Taylor, B.E., and Liou, J.G. (1978) The low-temperature stability of andradite in C-O-H fluids. American Mineralogist, 63, 378–393.

Tequì, C., Robie, R.A., Hemingway, B.S., Neuville, D.R., and Richet, P. (1991) Melting and thermodynamic properties of pyrope ($Mg_3Al_2Si_3O_{12}$). Geochimica et Cosmochimica Acta, 55, 1005–1010.

Tosi, M.P. (1964) Cohesion of ionic solids in the Born model. Solid State Physics, 16, 1–120.

Tosi, M.P., and Fumi, F.G. (1964) Ionic sizes and Born repulsive parameters in the NaCl-type alkali halides-II. Journal of Physical Chemistry of Solids, 25, 45–52.

Viellard, P. (1982) Modele de calcul des energies de formation des mineraux, bati sur la connaissance affinee des structures. Institut Geologie Université Louis Pasteur de Strasbourg, Memoire no. 69.

Weaver, J.S., Takahashi, T., and Bass, J.D. (1976) Isothermal compression of grossular garnets to 250 kbar and the effect of Ca on the bulk modulus. Journal of Geophysical Research, 81, 2476–2482.

Woodland, A.B., and Wood, B.J. (1989) Electrochemical measurement of the free energy of almandine ($Fe_3Al_2Si_3O_{12}$) garnet. Geochimica et Cosmochimica Acta, 53, 2277–2282.

Woodland, A.B., and O'Neill, H.St.C. (1993) Synthesis and stability of $Fe_3^{2+}Al_2Si_3O_{12}$-$Fe_3^{2+}Fe_2^{3+}Si_3O_{12}$ garnet and phase relations with $Fe_3^{2+}Al_2Si_3O_{12}$-$Fe_3^{2+}Fe_2^{3+}Si_3O_{12}$ solutions. American Mineralogist, 78, 1002–1015.

Woodland, A.B., and Ross, C.R., II (1994) A crystallographic and Mössbauer spectroscopy study of $Fe_3^{2+}Al_2Si_3O_{12}$-$Fe_3^{2+}Fe_2^{3+}Si_3O_{12}$ (almandine-"Skiagite") and $Ca_3Fe_2^{3+}Si_3O_{12}$-$Fe_3^{2+}Fe_2^{3+}Si_3O_{12}$ (andradite-"Skiagite") garnet solid solutions. Physics and Chemistry of Minerals, 21, 117–132.

Yagi, T., Akaogi, M., Shimamura, O., Tamai, H., and Akimoto, S. (1987) High pressure and high temperature equations of state of majorite. In M. Manghani and Y. Syono, Eds., High pressure research in mineral physics, p. 251–260. American Geophysical Union, Washington, DC.

Yakovlev, B.G., and Vozianova, O.V. (1983) The thermodynamic parameters of almandine. Geokhimiya, 1, 64–74.

Zemann, A., and Zemann, J. (1961) Verfeinerung der Kristallstructure von synthetischem Pyrope $Mg_3Al_2Si_3O_{12}$. Acta Crystallographica, 14, 835–837.

Zen, E. (1973) Thermochemical parameters of minerals from oxygen-buffered hydrothermal equilibrium data: method, application to annite and almandine. Contributions to Mineralogy and Petrology, 39, 65–80.

Zener, C. (1931) Interchange of translational, rotational and vibrational energy in molecular collisions. Physical Review, 37, 556–569.

Zhang, Z., and Saxena, S.K. (1991) Thermodynamic properties of andradite and application to skarn with coexisting andradite and hedenbergite. Contributions to Mineralogy and Petrology, 107, 255–263.

MANUSCRIPT RECEIVED MARCH 17, 1995
MANUSCRIPT ACCEPTED NOVEMBER 30, 1995